AFRL-RX-WP-TP-2011-4296

STRUCTURE OF CA-MG-ZN METALLIC GLASSES (PREPRINT)

O.N. Senkov

UES, Inc.

D.B. Miracle

Metals Branch
Metals, Ceramics, and NDE Division

E.B. Barney and A.C. Hannon

Rutherford-Appleton Laboratory

Y. Cheng and E. Ma

John Hopkins University

JULY 2011

AIR FORCE RESEARCH LABORATORY
MATERIALS AND MANUFACTURING DIRECTORATE
WRIGHT-PATTERSON AIR FORCE BASE, OH 45433-7750
AIR FORCE MATERIEL COMMAND
UNITED STATES AIR FORCE

REPORT DOCUMENTATION PAGE

Form Approved
OMB No. 0704-0188

1. REPORT DATE *(DD-MM-YY)*	2. REPORT TYPE	3. DATES COVERED *(From - To)*
July 2011	Journal Article Preprint	01 July 2011 – 01 July 2011

4. TITLE AND SUBTITLE
STRUCTURE OF CA-MG-ZN METALLIC GLASSES (PREPRINT)

5a. CONTRACT NUMBER
In-house

5b. GRANT NUMBER

5c. PROGRAM ELEMENT NUMBER
62102F

6. AUTHOR(S)
O.N. Senkov (UES, Inc.)
D.B. Miracle (AFRL/RXLM)
E.B. Barney and A.C. Hannon (Rutherford-Appleton Laboratory)
Y. Cheng and E. Ma (John Hopkins University)

5d. PROJECT NUMBER
4347

5e. TASK NUMBER
20

5f. WORK UNIT NUMBER
LM10512P

7. PERFORMING ORGANIZATION NAME(S) AND ADDRESS(ES)

UES, Inc.
Dayton, OH 45432-1894

Metals Branch (AFRL/RXLM)
Metals, Ceramics, and NDE Division
Air Force Research Laboratory, Materials and Manufacturing Directorate
Wright-Patterson Air Force Base, OH 45433-7750
Air Force Materiel Command, United States Air Force

Rutherford-Appleton Laboratory
ISIS Facility
Didcot, OX11 0QX, UK

John Hopkins University
Baltimore, MD 21218

8. PERFORMING ORGANIZATION REPORT NUMBER
AFRL-RX-WP-TP-2011-4296

9. SPONSORING/MONITORING AGENCY NAME(S) AND ADDRESS(ES)
Air Force Research Laboratory
Materials and Manufacturing Directorate
Wright-Patterson Air Force Base, OH 45433-7750
Air Force Materiel Command
United States Air Force

10. SPONSORING/MONITORING AGENCY ACRONYM(S)
AFRL/RXLM

11. SPONSORING/MONITORING AGENCY REPORT NUMBER(S)
AFRL-RX-WP-TP-2011-4296

12. DISTRIBUTION/AVAILABILITY STATEMENT
Approved for public release; distribution unlimited.

13. SUPPLEMENTARY NOTES
PAO Case Number: 88ABW 2010-2103; Clearance Date: 16 Apr 2010. Document contains color.
Journal article submitted to *Metallurgical and Materials Transactions A.*

14. ABSTRACT
The amorphous structure of four $Ca_{60}Mg_XZn_{40-X}$ alloys (X = 10, 15, 20, and 25 at.%) has been modeled using a set of experimental neutron and X-ray scattering data, peak fit analysis, and Reverse Monte Carlo (RMC) simulation. The amorphous structure can be described as a mixture of Mg- and Zn- centered clusters, with Ca dominating in the first coordination shell of these clusters. The coordination number (CN) of 10 (with about 7 Ca and 3 (Mg+Zn) atoms) is the most common for the Zn-centered clusters. CN = 11 and 12 (with about 7-8 Ca and 4 (Mg+Zn) atoms) are the most common for the Mg-centered clusters. Fife-fold bond configurations (pentagonal pyramids) dominate (~60%) in the first coordination shell of the clusters, suggesting densely atomic packing. Bond angle distributions suggest the near-equilateral triangles and pentagonal pyramids to be the most common nearest atom configurations. Two Ca-Mg-Zn alloys with inferior GFA have increased amounts of (0,0,12,0), (0,2,8,1), (0,2,8,2) and (0,4,4,3) clusters, which suggests that these clusters may facilitate crystallization.

15. SUBJECT TERMS
$Ca_{60}Mg_XZn_{40-X}$ alloys, pentagonal pyramids, bulk metallic glasses (BMGs)

16. SECURITY CLASSIFICATION OF:			17. LIMITATION OF ABSTRACT:	18. NUMBER OF PAGES	19a. NAME OF RESPONSIBLE PERSON (Monitor)
a. REPORT	b. ABSTRACT	c. THIS PAGE			Jonathan E. Spowart
Unclassified	Unclassified	Unclassified	SAR	50	19b. TELEPHONE NUMBER *(Include Area Code)* N/A

STRUCTURE OF CA-MG-ZN METALLIC GLASSES

O.N. Senkov,[1,2,*] D.B. Miracle,[1] E.B. Barney,[3] A.C. Hannon,[3] Y. Cheng,[4] E. Ma [4]

[1] Air Force Research Laboratory, Materials and Manufacturing Directorate, Wright-Patterson Air Force Base, Ohio 45433, USA

2 UES, Inc., Dayton, Ohio 45432, USA

[3] ISIS Facility, Rutherford-Appleton Laboratory, Didcot, OX11 0QX, UK

[4] John Hopkins University, Baltimore, MD 21218, USA

ABSTRACT

The amorphous structure of four $Ca_{60}Mg_XZn_{40-X}$ alloys (X = 10, 15, 20, and 25 at.%) has been modeled using a set of experimental neutron and X-ray scattering data, peak fit analysis, and Reverse Monte Carlo (RMC) simulation. The amorphous structure can be described as a mixture of Mg- and Zn- centered clusters, with Ca dominating in the first coordination shell of these clusters. The coordination number (CN) of 10 (with about 7 Ca and 3 (Mg+Zn) atoms) is the most common for the Zn-centered clusters. CN = 11 and 12 (with about 7-8 Ca and 4 (Mg+Zn) atoms) are the most common for the Mg-centered clusters. Fife-fold bond configurations (pentagonal pyramids) dominate (~60%) in the first coordination shell of the clusters, suggesting densely atomic packing. Bond angle distributions suggest the near-equilateral triangles and pentagonal pyramids to be the most common nearest atom configurations. Two Ca-Mg-Zn alloys with inferior GFA have increased amounts of (0,0,12,0), (0,2,8,1), (0,2,8,2) and (0,4,4,3) clusters, which suggests that these clusters may facilitate crystallization.

[*] Corresponding author. Phone 1-937-255-1320; Fax: 1-937-656-7292; e-mail: oleg.senkov@wpafb.af.mil.

INTRODUCTION

Recently discovered ternary Ca-Mg-Zn, Ca-Mg-Cu and Ca-Mg-Al bulk metallic glasses (BMGs) have unique properties, which distinguish them from other BMGs [1,2,3,4,5]. They are based on two simple elements, Ca and Mg, and have the lowest density (in the range of 1.6 – 2.4 g/cm^3) among all currently known BMGs [6]. These metallic glasses also have extremely low Young's (~20-30 GPa) and shear moduli (~9-14 GPa), comparable with the moduli of human bones [7]. Some of these ternary alloys have extremely good glass forming ability (GFA), similar to GFA of the best Pd- and Zr- based BMGs [4,6,8].

Figure 1 shows the Ca-rich corner of the liquidus projection of the Ca-Mg-Zn system [9]. The compositions of the ternary Ca-Mg-Zn ternary amorphous alloys reported in [2,4] are marked as solid circles and their critical plate thicknesses are shown by corresponding numbers (in mm). The presence of the ternary eutectic reaction provides a strong liquidus temperature gradient in the selected composition area, which leads to high sensitivity of GFA with alloy composition. For example, the maximum plate thickness at which an alloy is fully amorphous after casting in a water-cooled copper mold, can be increased by more than 10 times, from 0.5 mm to 6-10 mm, within only 5% composition range [4]. Thermodynamic analysis of the onset driving force (ODF) for crystallization of different phases in the Ca-Mg-Zn system has clearly shown [10] that GFA of the ternary alloys improves with a decrease in the ODF of competing phases. For example, amorphization of $Ca_{60}Mg_XZn_{40-X}$ alloys competes with crystallization of CaZn (at $X \leq$ 17.5at%) and $CaMg_2$ (at X > 17.5 at.%) phases (Figure 2).

Based on relative atomic sizes [11] and the efficient solute-centered cluster packing (ECP) model of amorphous structure [12] the Ca-Mg-Zn ternary glasses are represented as <10,9> efficient cluster packing structures, where Mg solutes are surrounded by ~10 nearest neighbors

and Zn solutes have ~9 nearest neighbors, assuming that all the nearest neighbors are solvent atoms (i.e. Ca). Glass compositions predicted from the ECP model range from $Ca_{70}Mg_{15}Zn_{15}$ to $Ca_{53}Mg_{12}Zn_{35}$ [13], which fit within the trapezoid shown in Figure 1.

The current work is aimed at studying the amorphous structure of a series of ternary $Ca_{60}Mg_XZn_{40-X}$ (X = 10, 15, 20, 25 at.%) metallic glasses with the use of neutron and X-ray scattering and Reverse Monte Carlo (RMC) modeling and relating this structure to the alloy compositions and GFA. The amorphous structure identified in this work is compared with the amorphous structure predicted by the ECP model [12].

EXPERIMENTAL PROCEDURES

Sample Preparation

Four amorphous alloys, $Ca_{60}Mg_{10}Zn_{30}$, $Ca_{60}Mg_{15}Zn_{25}$, $Ca_{60}Mg_{20}Zn_{20}$, and $Ca_{60}Mg_{25}Zn_{15}$, were used in this study. Among these, the $Ca_{60}Mg_{10}Zn_{30}$ and $Ca_{60}Mg_{25}Zn_{15}$ alloys show marginal GFA, with the maximum fully-amorphous plate thicknesses achievable during water-cooled copper mold casting of 0.5 mm and 1 mm, respectively [2,4]. Two other alloys, $Ca_{60}Mg_{15}Zn_{25}$ and $Ca_{60}Mg_{20}Zn_{20}$ are better bulk glass formers and their maximum fully amorphous plate thicknesses were identified to be 6 mm and 4 mm, respectively. In order to exclude the casting condition effects, the amorphous specimens of all four alloys were prepared by the same method of melt spinning in the form of ~0.2 mm thick ribbons. Prior to the neutron and X-ray diffraction analysis, these ribbons were ground into powder. The density ρ_o of the amorphous alloys was measured with a helium pycnometer AccuPyc 1330 V1.03 and the values (in g/cm^3 and atoms/Å^3) are given in Table 1. The following formula was used for the density conversion:

$$\boldsymbol{\rho_o[\text{atoms/Å}^3] = (N_A/\sum c_i A_i)\, \rho_o[\text{g/cm}^3]}, \quad (1)$$

where N_A is the Avogadro's number and c_i and A_i are the atomic fraction and atomic mass, respectively of the element *i* (Ca, Mg or Zn) in a given alloy.

Neutron and X-ray Scattering

The neutron scattering experiments were conducted at room temperature in vacuum using a General Materials (GEM) diffractometer at the ISIS high-intensity pulsed neutron source (Rutherford Appleton Laboratory, Didcot, UK). The GEM detector has eight banks to collect the data within the Q range from 0.1 to 100 Å^{-1}, where Q is the scattering vector of length $4\pi\sin\Theta/\lambda$ for a neutron of wavelength λ scattered at an angle 2Θ. The exposure time for each specimen was about 210 min, which corresponded to the accumulated intensity of ~5.7×10^6 scattered neutrons. The X-ray scattering experiments were conducted at room temperature in argon atmosphere on Panalytical Xpert-PRO diffractometer (ISIS facility) using Ag radiation. The useful Q range was from 0.5 to 18 Å^{-1}.

The ISIS developed software, Gudrun and GudrunX, were used to process the neutron and X-ray scattering data and obtain the experimental total scattering structure factors *S(Q)* and $S^x(Q)$, as well as total radial distribution functions (RDFs) *G(r)* and $G^x(r)$. The superscript '*x*' indicates that the data was obtained by X-ray scattering. These functions are related to the partial radial distribution functions (PRDFs), $g_{ij}(r)$, as follow [14]:

$$S(Q) = \frac{4\pi\rho_o}{Q}\sum_{i,j=1}^{3} c_i c_j b_i b_j \int_0^\infty r\left[g_{ij}(r)-1\right]\sin(Qr)dr \qquad (2)$$

$$S^x(Q) = \frac{4\pi\rho_o}{Q}\sum_{i,j=1}^{3} c_i c_j \frac{f_i(Q) f_j(Q)}{\sum_{i=1}^{3} c_i f_i(Q)^2}\int_0^\infty r\left[g_{ij}(r)-1\right]\sin(Qr)dr \qquad (3)$$

$$G(r) = \sum_{i,j=1}^{3} c_i c_j b_i b_j \left[g_{ij}(r)-1\right] \qquad (4)$$

$$G^x(r) = \sum_{i,j=1}^{3} \frac{c_i c_j Z_i Z_j}{\left(\sum_{i=1}^{3} c_i Z_i\right)^2} \left[g_{ij}(r) - 1\right] \quad (5)$$

In Equations (2) through (5), c_i, b_i, $f_i(Q)$ and Z_i are, respectively, the atomic fraction, coherent bound neutron scattering length, X-ray scattering factor and atomic number of element *i* (Ca, Mg, or Zn), ρ_o is the average number density of the material (in atoms per $Å^3$), and *r* is a distance from an arbitrary point in the amorphous structure.

Reverse Monte Carlo Simulation

The three-dimensional models of the amorphous structures of the Ca-Mg-Zn alloys, which agree with the experimental data, boundary conditions and coordination constraints, were generated with the use of the Reverse Monte Carlo (RMC) simulation technique described in details in [15].The simulation boxes with periodic boundary conditions contained from1600 to 4000 atoms. The input data used in this simulation were the experimental neutron and X-ray total structure factors, $S(Q)$ and $S^x(Q)$, and radial distribution functions, $G(r)$. The main coordination constraints used in this work were the fixed alloy density and excluded volume (minimum interatomic distances). These two constraints were found to improve the separation of partials in cases where the separation matrix is poorly conditioned [15,16]. Because the dominant effect determining the amorphous structure is the atomic packing, included information on the atomic bond distances in the model severely limited the number of structures that were consistent with the experimental data. The bond distances were estimated from the available data for $CaMg_2$, Ca_3Zn, Ca_5Zn_3, CaZn, and $MgZn_2$ intermetallics [17]. Two additional coordination constraints were also used during initial stages of the simulations, Additional assumptions that (a) the average nearest bond distances between six pair atoms (Ca-Ca, Ca-Mg, Ca-Zn, Mg-Mg, Mg-Zn,

and Zn-Zn) are the same in four studied alloys and (b) the nearest atom-pair bond distributions are described by Gaussian functions, were also used during the first stages of simulation.

The RMC computed amorphous structures were analyzed with the use of special programs, which allow calculation of PRDFs, type and distribution of coordination polyhedra (atomic clusters), neighbor coordination numbers, triplet angle correlations, etc.

RESULTS

Pair Correlations

The eventual matches between the RMC simulated and experimental total scattering factors and radial distribution functions after ~10^7 RMC steps are demonstrated in

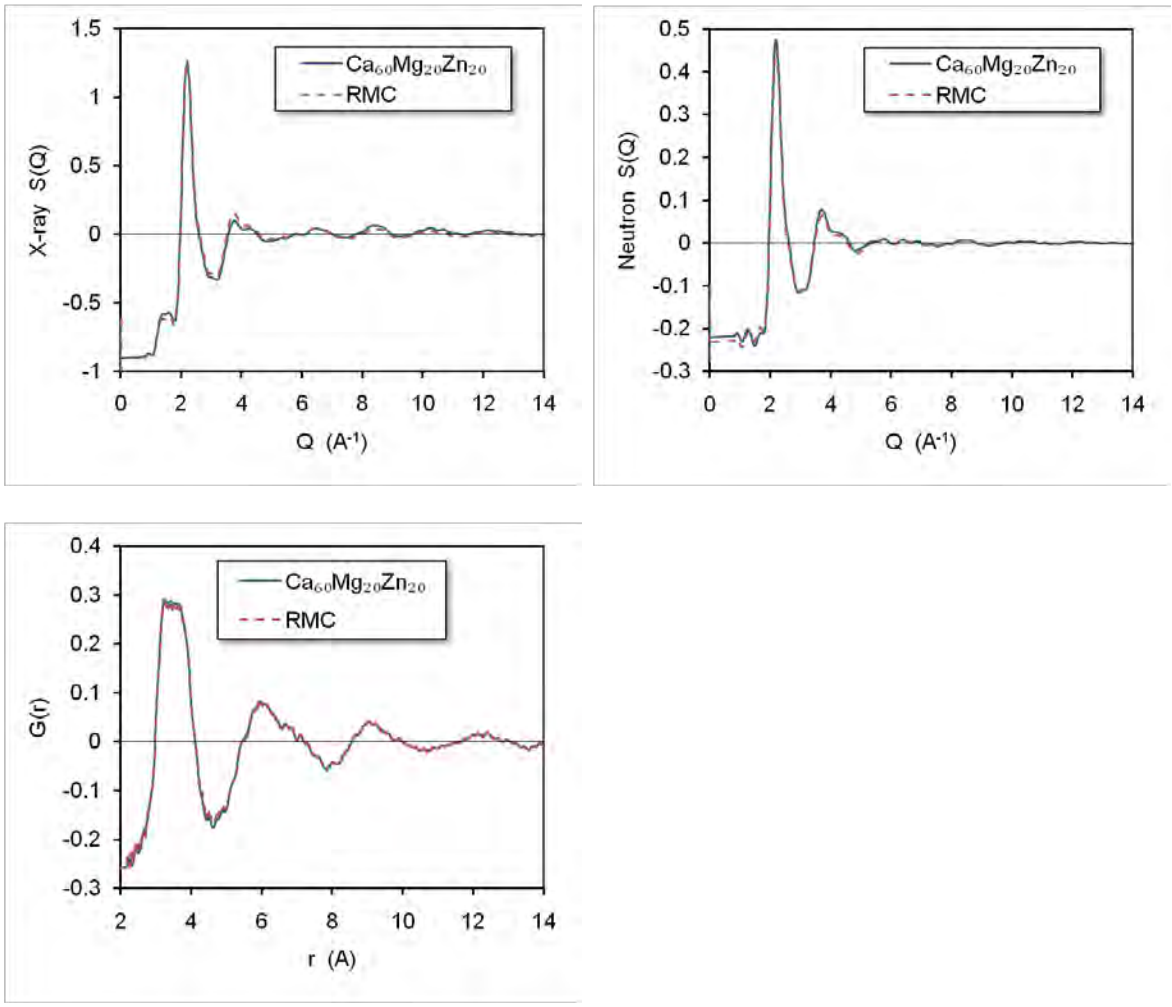

Figure 3. An excellent fit indicates that the RMC-simulated amorphous structure describes the experimental spectra very well. The first G(r) peak located in the r-range between 2.21 and 4.6 Å, corresponds to positions between atoms within the first coordination shell. Six PRDFs corresponding to the simulated amorphous structure are shown in

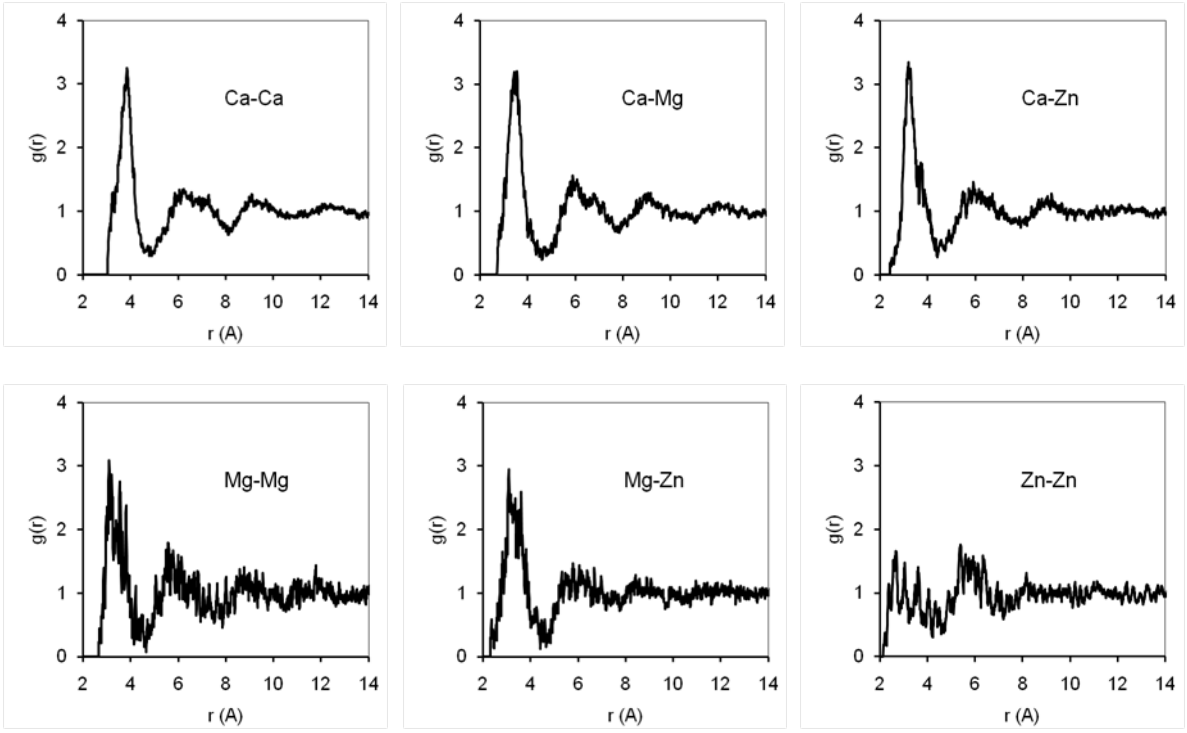

Figure 4. A single $g_{ij}(r)$ peak inside the first coordination shell range is clearly seen in Ca-Ca, Ca-Mg, and Ca-Zn PRDFs, and the bond distances r_{ij} between the Ca-Ca, Ca-Mg, and Ca-Zn pairs corresponding to this peak are identified to be 3.84 Å, 3.48 Å, and 3.21 Å, respectively. On the other hand, the Mg-Mg, Mg-Zn and, especially, Zn-Zn bond distances within the first shell (i.e. inside the first RDF peak) are not defined by a single $g_{ij}(r)$ peak. Instead, several $g_{ij}(r)$ peak positions are common (see

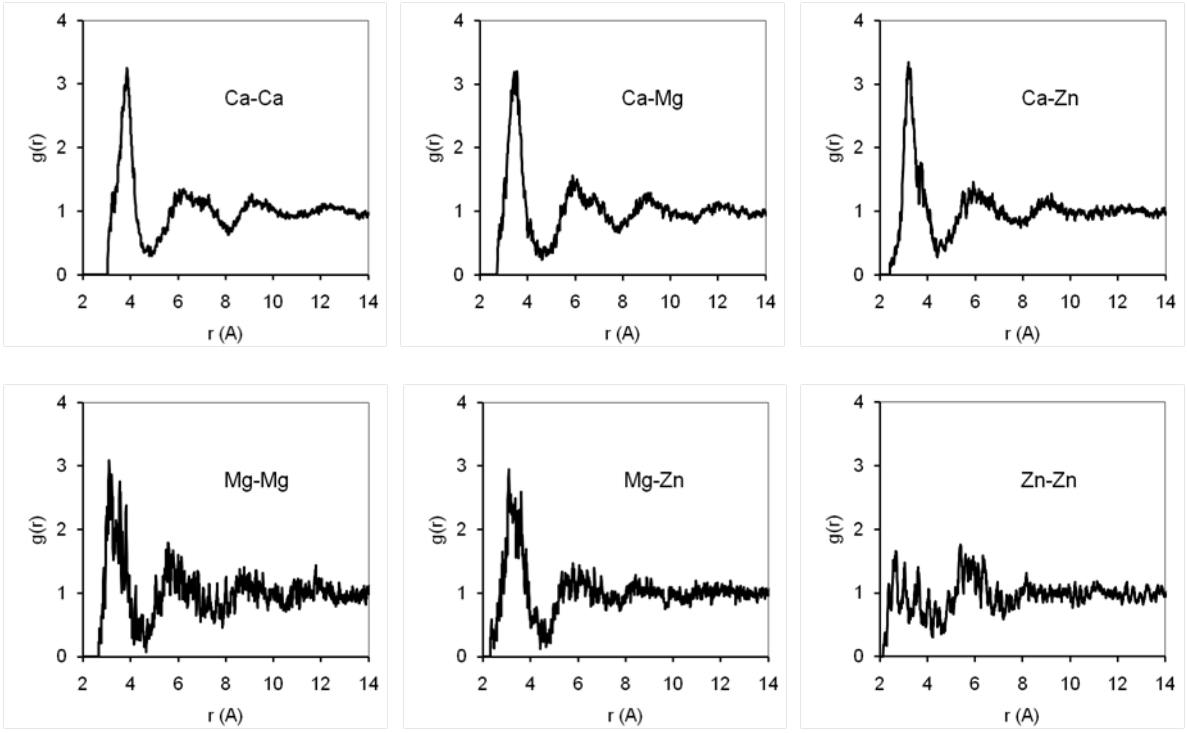

Figure 4). For example, three $g_{MgMg}(r)$ peaks are seen within the first coordination shell corresponding to the characteristic Mg-Mg bond distances of 3.02 Å, 3.54 Å and 3.80 Å. For the Zn-Zn PRDF, four peaks, at r_{MgMg} = 2.63 Å, 3.05 Å, 3.61 Å and 4.04 Å, are present within the first shell. Similar behavior of PRDFs has also been noticed for other three Ca-Mg-Zn amorphous alloys.

The inter-atomic bond distances calculated from the position of the first peak of respective PRDfs for four Ca-Mg-Zn amorphous alloys are given in Table 2. These calculated r_{ij} are about 2.3 – 4.1 % smaller than the respective metallic bond distances, r_m, and about 6.5 – 9.8% larger than the respective covalent bond distances, r_c (see Table 3). Using the lever rule,

$$f_c = (r_m - r_{ij})/(r_m - r_c) \quad (7)$$

the covalent fraction of bonds, f_c, was determined for six atomic pairs in four studied amorphous alloys. The results are given in Table 4. It can be noticed that the Ca-Zn bonds are noticeably shorter and Zn-Zn bonds are longer in marginal glasses ($Ca_{60}Mg_{10}Zn_{30}$ and $Ca_{60}Mg_{25}Zn_{15}$) than in good bulk glass formers ($Ca_{60}Mg_{15}Zn_{25}$ and $Ca_{60}Mg_{20}Zn_{20}$).

Table 5 provides characteristic first-shell bond distances between Ca, Mg, and Zn atom pairs in several binary intermetallics. The crystal structure constraints lead to discrete values of the bond distances in these intermetallics. It can be seen that the $r_{Ca\text{-}Mg}$ and $r_{Zn\text{-}Mg}$ values in the amorphous Ca-Mg-Zn alloys given in Table 2 are smaller than the respective interatomic distance in the crystalline intermetallic phases, while other r_{ij} in the amorphous alloys are close to the minimum r_{ij} values in the crystalline intermetallics. This observation may indicate that the absence of long range order constraints leads to shortening the interatomic distances between the nearest neighbor atoms in the amorphous structure, as compared to the binary intermetallics.

Weighted bond distances, $r_{ij}^{weighted}$, between the atom pairs within the first peak of the total RDFs of the Ca-Mg-Zn amorphous alloys are given in Table 6. They are calculated using the following equation:

$$r_{ij}^{weighted} = \int_{r_1}^{r_2} r g_{ij}(r) dr \Big/ \int_{r_1}^{r_2} g_{ij}(r) dr \qquad (8)$$

where r_1 and r_2 are the minimum and maximum cut-offs for the first shell. When the values in Table 6 are compared with respective values in Table 2, it can be found that $r_{ij}^{weighted}$ are always higher than the first peak r_{ij} values. The difference increases with a decrease in the size of pair atoms.

The clearly identified single PRDF peak for Ca-Ca, Ca-Mg and Ca-Zn atom pairs within the first coordination shell may indicate that the atoms in these pairs attract each other and are touching

each other. On the other hand, Mg-Mg, Mg-Zn and, especially, Zn-Zn pairs are less attractive to each other. As a result, Mg- and Zn- centered atoms prefer to have Ca atoms as the nearest neighbors in the first shell and the first-shell Mg and Zn atoms just fill gaps between the Ca atoms, so that their distances from the center atom (Mg or Zn) vary depending on the gap values. This observation also indicates that Zn atoms like to be more separated than other atoms.

Coordination Polyhedra and Coordination Numbers

Atoms in metallic glasses tend to arrange themselves so as to maximize the local packing density[12,18 ,24] and the finite sizes of atoms impose geometrical restrictions on the possible local atom environments [19]. The local environment of an atom *i* is generally treated in terms of the geometry of the shell formed by its nearest neighbor atoms [23,20]. The chemistry (i.e. the number of different atom species and their relative positions) of the first coordination shell provide additional important information about the local environment.

Interatomic bonds in metallic glasses are generally non-directional, and the nearest neighbors for any chosen atom *i* are often defined as atoms, which are in contact with *i* or separated from it by a distance smaller than a certain threshold value. The latter is defined globally as the position of the first minimum of RDF of the whole atomic array and, therefore, this approach is not sensitive to the details of the first shell geometry and to local density and chemistry fluctuations.

Another, more advanced, approach is to define the nearest neighbors as atoms that have common faces in their Voronoi polyhedra [18]. This definition of the first coordination shell atoms is straightforward and reflects the local details of the atomic packing topology. In this approach, a *coordination polyhedron* with the vertices located in positions of the first coordination shell atoms and with the edges coinciding with the interatomic bonds is defined for any chosen atom *i* [23]. Each coordination polyhedron, which is also called an *i*-centered cluster [12,21], is

assigned a characteristic Voronoi signature (v_3,v_4,v_5,v_6), where v_m is the number of the vertices (first coordination shell atoms) with *m* entering edges/bonds [22] (*m* is also called the vertex coordination.) The *i*-centered clusters with the same Voronoi signature are considered to be topologically equivalent (even if they are not identical) because they can be transformed into each other by 'elastic' deformation without changing the number of all vertices and connecting edges. In addition to assigning the topology, the Voronoi signature also defines the total coordination number (CN) of the cluster as CN = $\sum v_m$. The same Voronoi signature clusters can however be chemically different if they consist of different elements. Therefore, in addition to the Voronoi signature, partial coordination numbers, i.e. the number of atoms of different species, should also be known for a more complete description of the short range order in the amorphous structure.

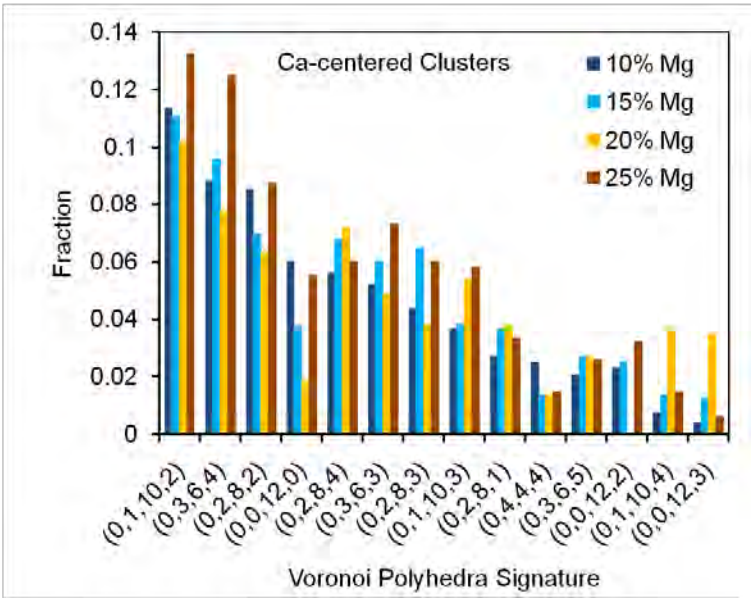

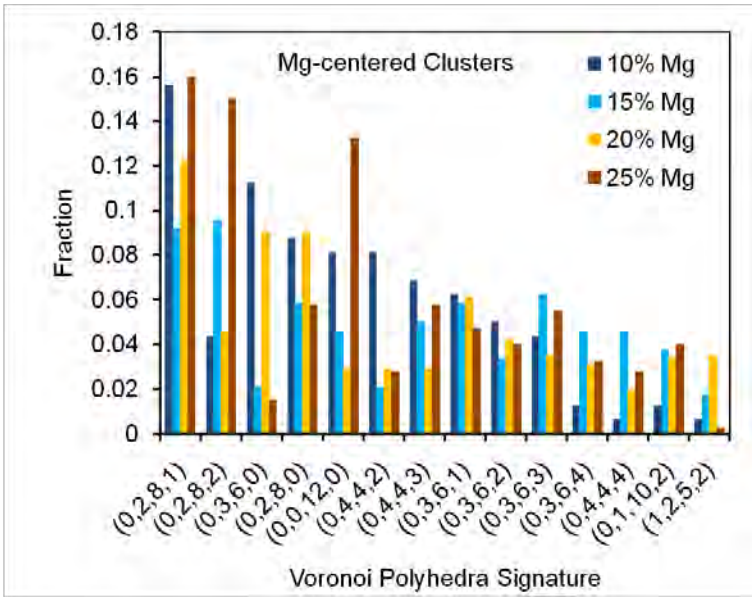

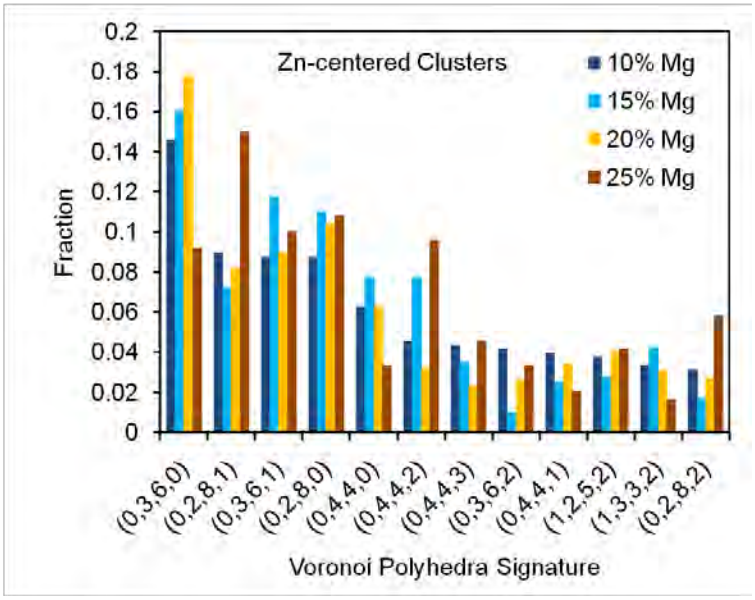

Figure 5 illustrates types and fractions of Ca-, Mg- and Zn- centered coordination polyhedra found in the amorphous structures of four Ca-Mg-Zn alloys. Although many types of the coordination polyhedra are presented in the amorphous structures, the most populated clusters can be identified. These are (0,1,10,2) for Ca-centered, (0,2,8,1) for Mg-centered and (0,3,6,0),

(0,2,8,1), (0,3,6,1) and (0,2,8,0) for Zn-centered clusters. Three examples of the clusters extracted from the amorphous structures are given in

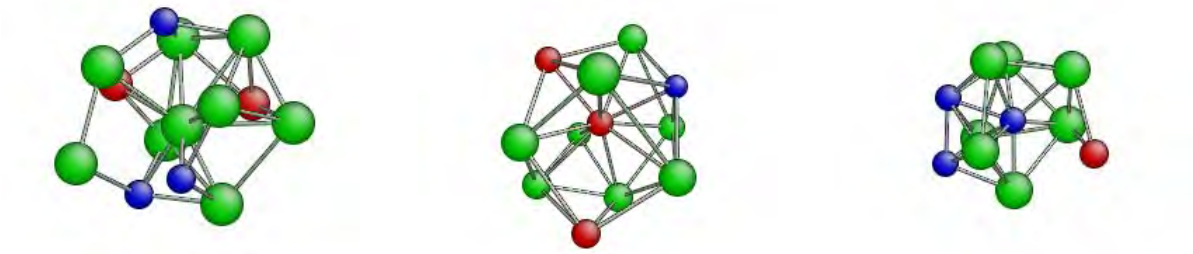

(a) (b) (c)

Figure 6. It can be noticed from

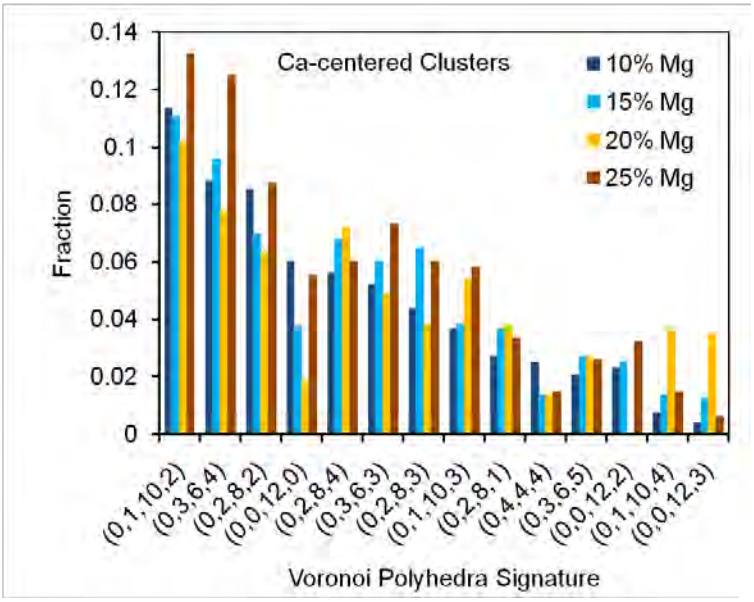

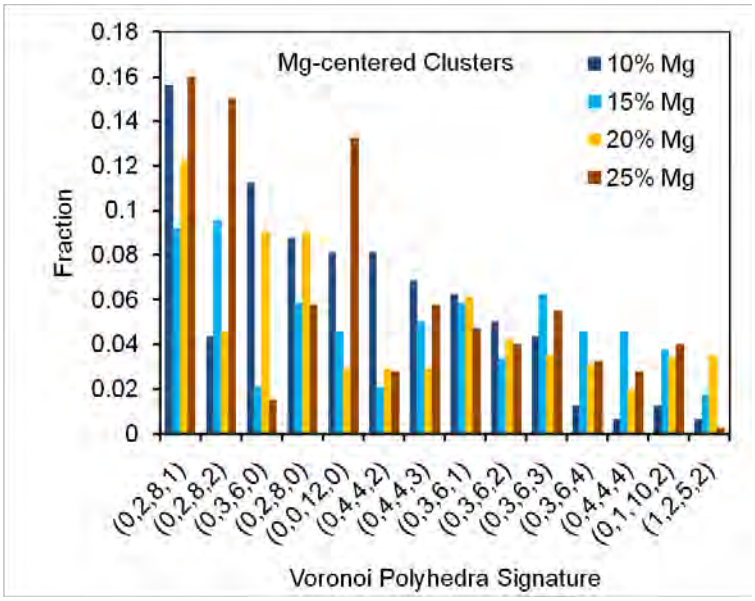

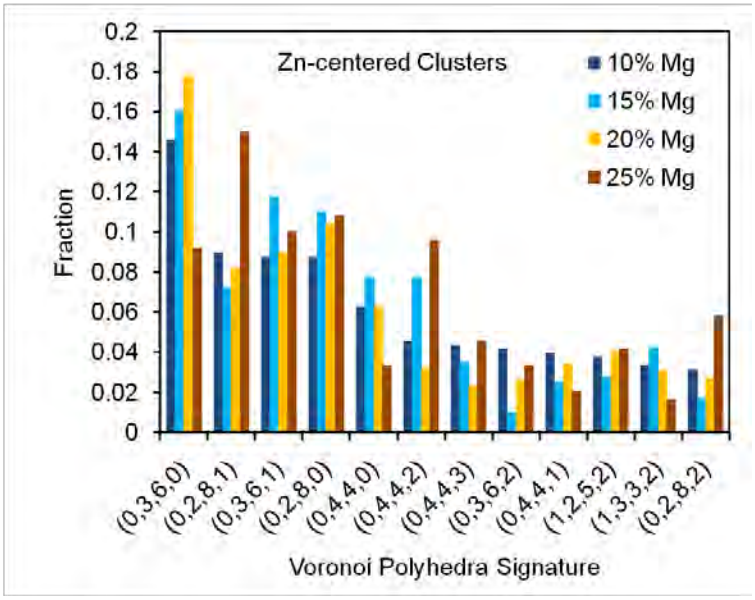

Figure 5 that the marginal glass forming alloys (with 10% and 25% Mg) have an increased fraction of (0,0,12,0), (0,2,8,1), (0,2,8,2) and (0,4,4,3) clusters in comparison with the good glass forming alloys (with 15% and 20% Mg). It is likely that these clusters facilitate crystallization during solidification thus reducing glass forming ability.

Though the amorphous structures of $Ca_{60}Mg_XZn_{40-X}$ alloys contain many types of the first-shell clusters, the competing crystal phases, $CaMg_2$ and CaZn, [10] contain only three and two types of the clusters, respectively. For example,

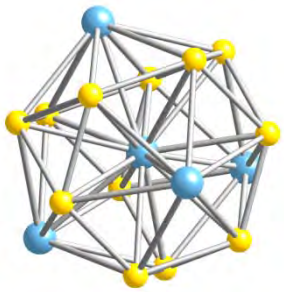

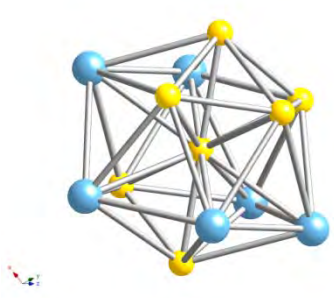

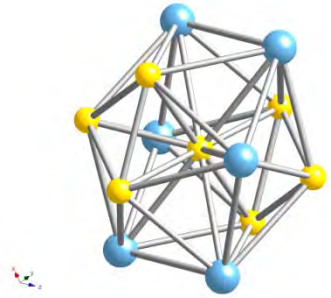

(a) (b) (c)

Figure 7 shows three principal clusters (one is the Ca-centered and two are Mg-centered) presented in the $CaMg_2$ intermetallic phase, and (a)

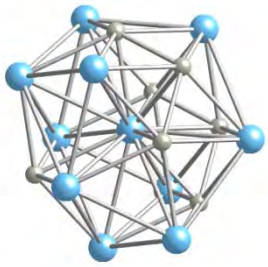

(b)

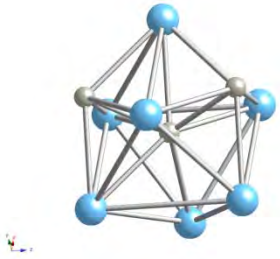

Figure 8 shows two clusters (Ca- and Zn- centered) presented in the CaZn intermetallic phase. The Ca-centered clusters, (0,0,12,4) in $CaMg_2$ and (0,1,10,6) CaZn, are not presented in the analyzed amorphous structures. The two Mg-centered clusters in $CaMg_2$ are (0,0,12,0) and the Zn-centered cluster in CaZn is (0,3,6,0). Similar Mg- and Zn- centered clusters are also populated in the amorphous structures (see

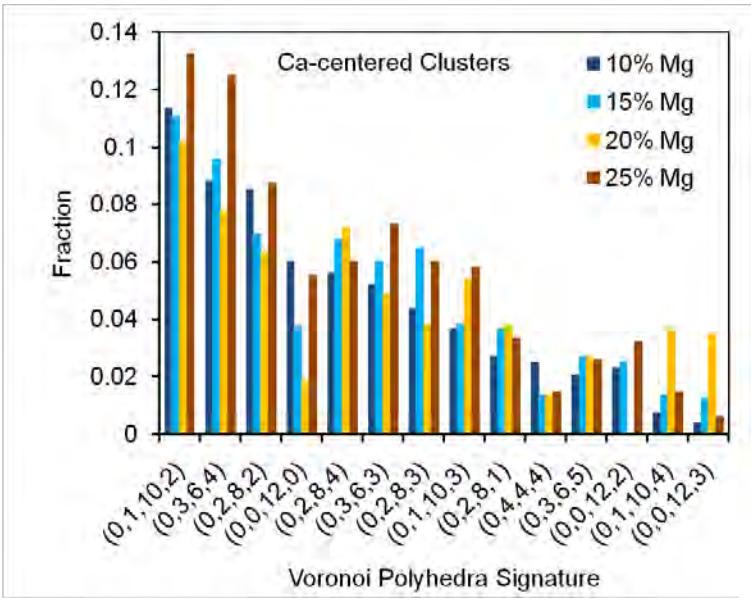

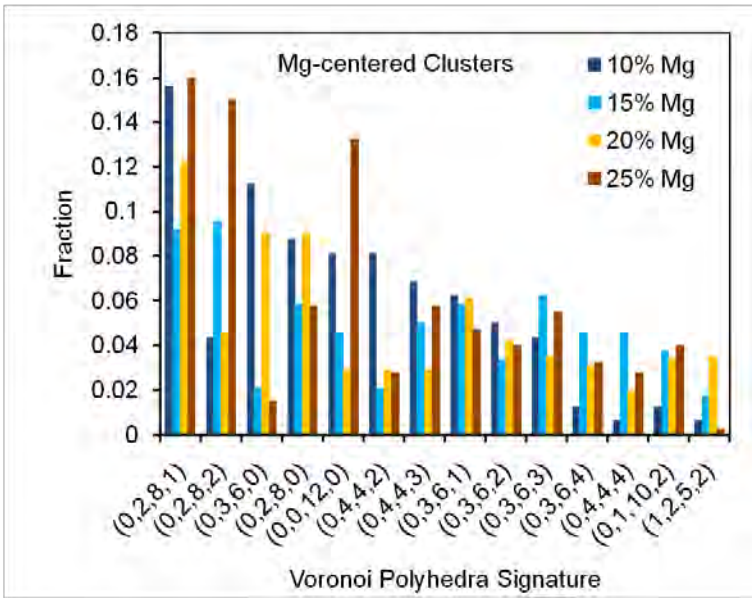

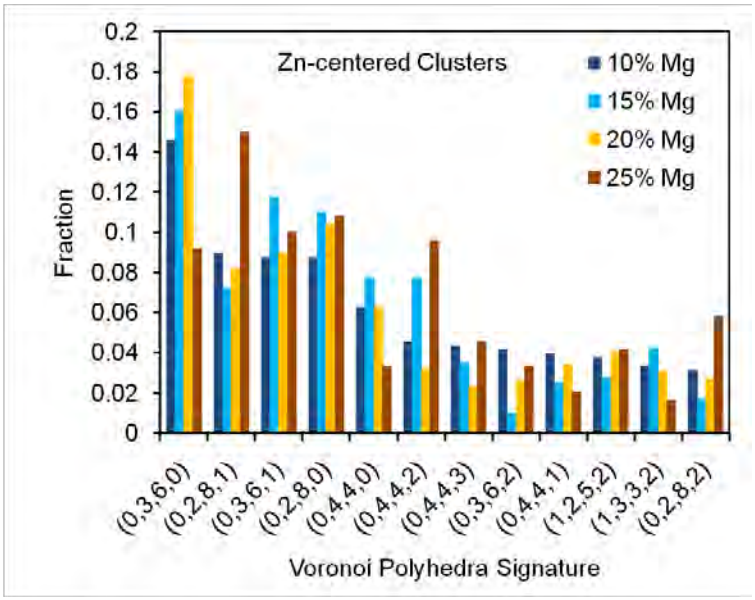

Figure 5).

The distributions of the atomic clusters by the total coordination numbers (CN) in the first shell are shown in

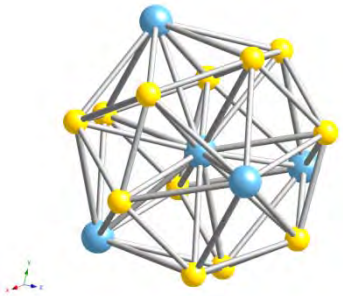

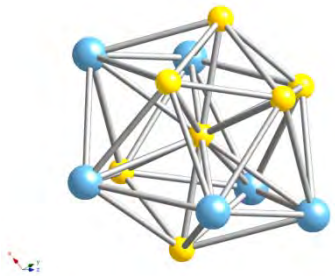

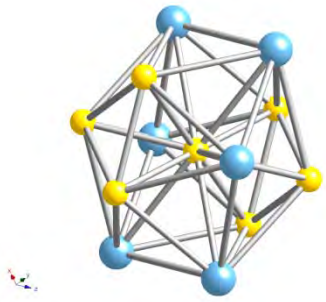

(a) (b) (c)

Figure 7. (a) Ca-centered (0,0,12,4) and (b, c) Mg-centered, both are (0,0,12,0), coordination polyhedra in the $CaMg_2$ crystal structure.

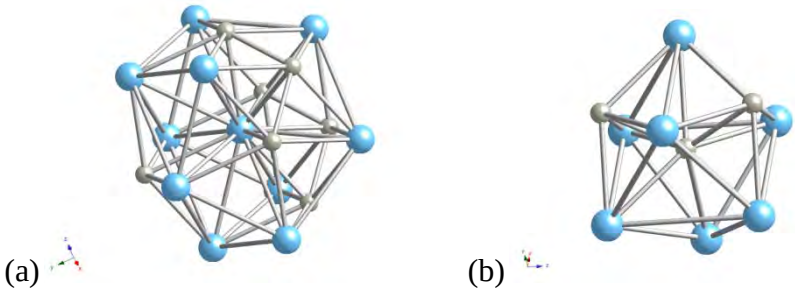

Figure 8. (a) Ca-centered (0,1,10,6) and (b) Zn-centered (0,3,6,0) coordination polyhedra in the CaZn crystal structure. []

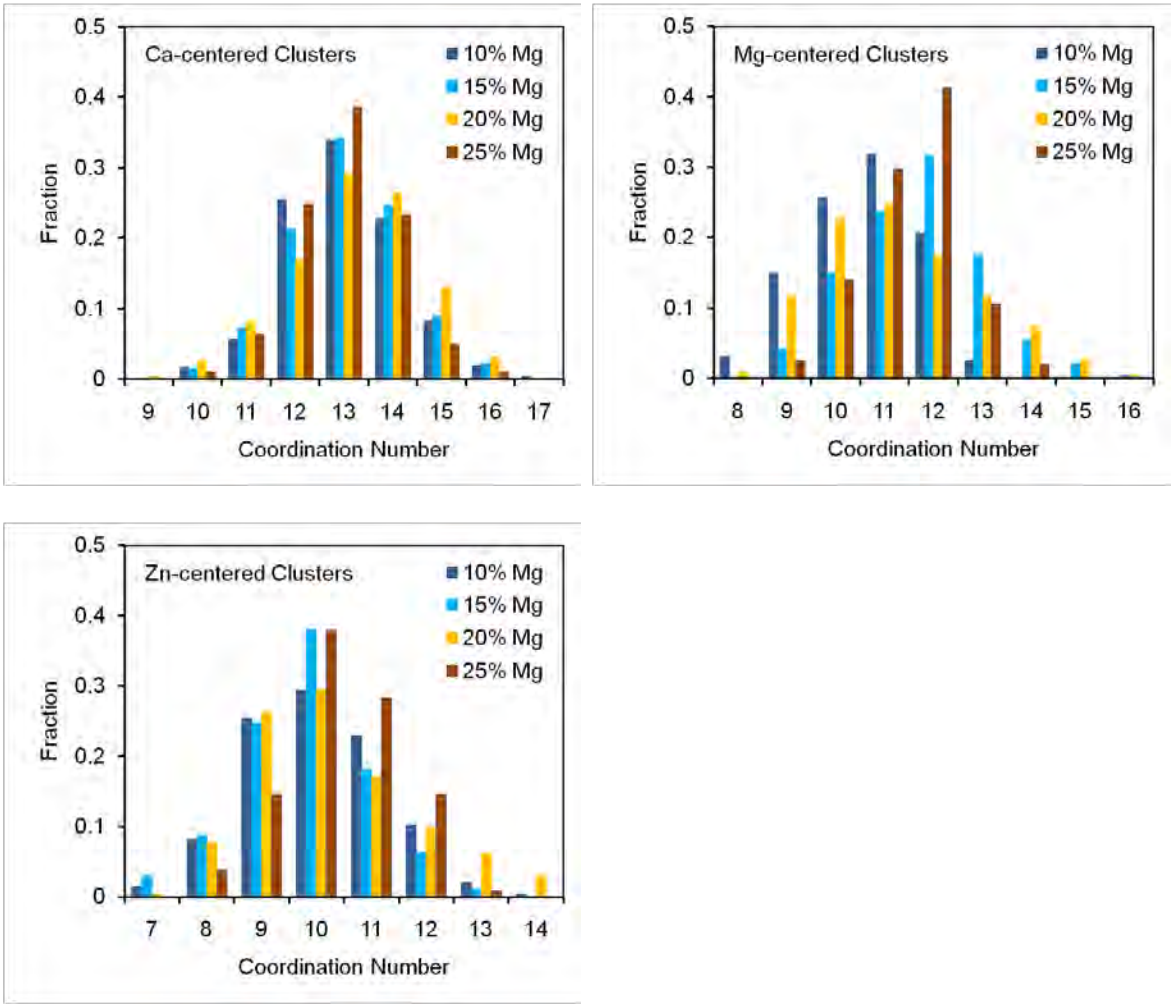

Figure 9 for the $Ca_{60}Mg_XZn_{40-X}$ amorphous alloys. There is no notable difference in the distributions between good (X = 15 and 20) and marginal (X = 10 and 25) glass formers. The most populated coordination numbers are CN = 13 for the Ca-centered clusters, CN = 11 and 12 for Mg-centered clusters and CN = 10 for Zn-centered clusters. The CN values for the Zn- and Mg- centered clusters are higher than the CN values of 9 and 10, expected for these clusters from the densely-packed solute-centered cluster (DPSCC) model [12]. This discrepancy is most likely due to the fact that the DPSCC model assumes that only solvent (Ca) atoms are presented in the first coordination shell. However, if some Ca atoms are replaced by the smaller Mg and Zn atoms, larger number of atoms is expected in the first shell.

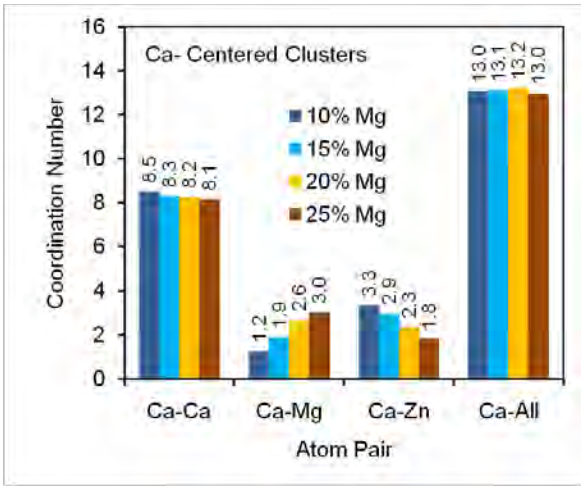

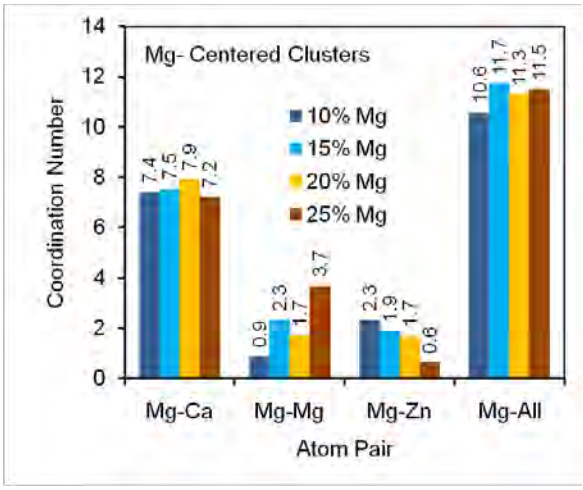

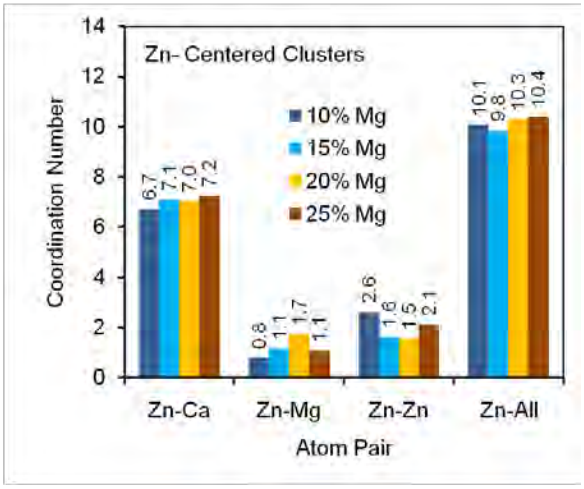

Figure 10 shows the average number of Ca, Mg, and Zn atoms in the first shell of the Ca-, Mg-, and Zn- centered clusters in the Ca-Mg-Zn amorphous alloys. It can be seen that the Ca atoms prevail in the first shell of the clusters and an increase in the concentration of Mg from 10 to 25% almost does not affect the number of Ca atoms in all three kind clusters. The respective Ca-Ca, Mg-Ca and Zn-Ca partial coordination numbers (PCN) are $PCN_{Ca\text{-}Ca}$ = 8.1-8.5, $PCN_{Mg\text{-}Ca}$ = 7.2-7.9, and $PCN_{Zn\text{-}Ca}$ = 6.7-7.2. At the same time, the number of Mg atoms increases (i.e. $PNC_{Ca\text{-}Mg}$ increases from 1.2 to 3.0 and $PNC_{Mg\text{-}Mg}$ increases from 0.9 to 3.7) and the number of Zn atoms decreases ($PNC_{Ca\text{-}Zn}$ decreases from 3.3 to 1.8 and $PNC_{Mg\text{-}Zn}$ decreases from 2.3 to 0.6) in the Ca- and Mg- centered clusters with an increase in the concentration of Mg. The amount of Zn and Mg in the Zn-centered glasses is mainly dependent on the type of glasses than on the amount of Mg in the alloys. Namely, marginal glasses (with 10% and 25% Mg) have an increased amount of Zn and a decreased amount of Mg in Zn-centered clusters than good glass-forming alloys (with 15% and 20% Mg).

The neighbor environment of a specific *j* atom in the first coordination shell of an *i*-centered cluster can be described by the vertex coordination number m_j, i.e. the number of the *j* atom

neighbors located in the first shell of the *i*-centered cluster [23,24] or the number of edges (bonds) entering the vertex *j*.

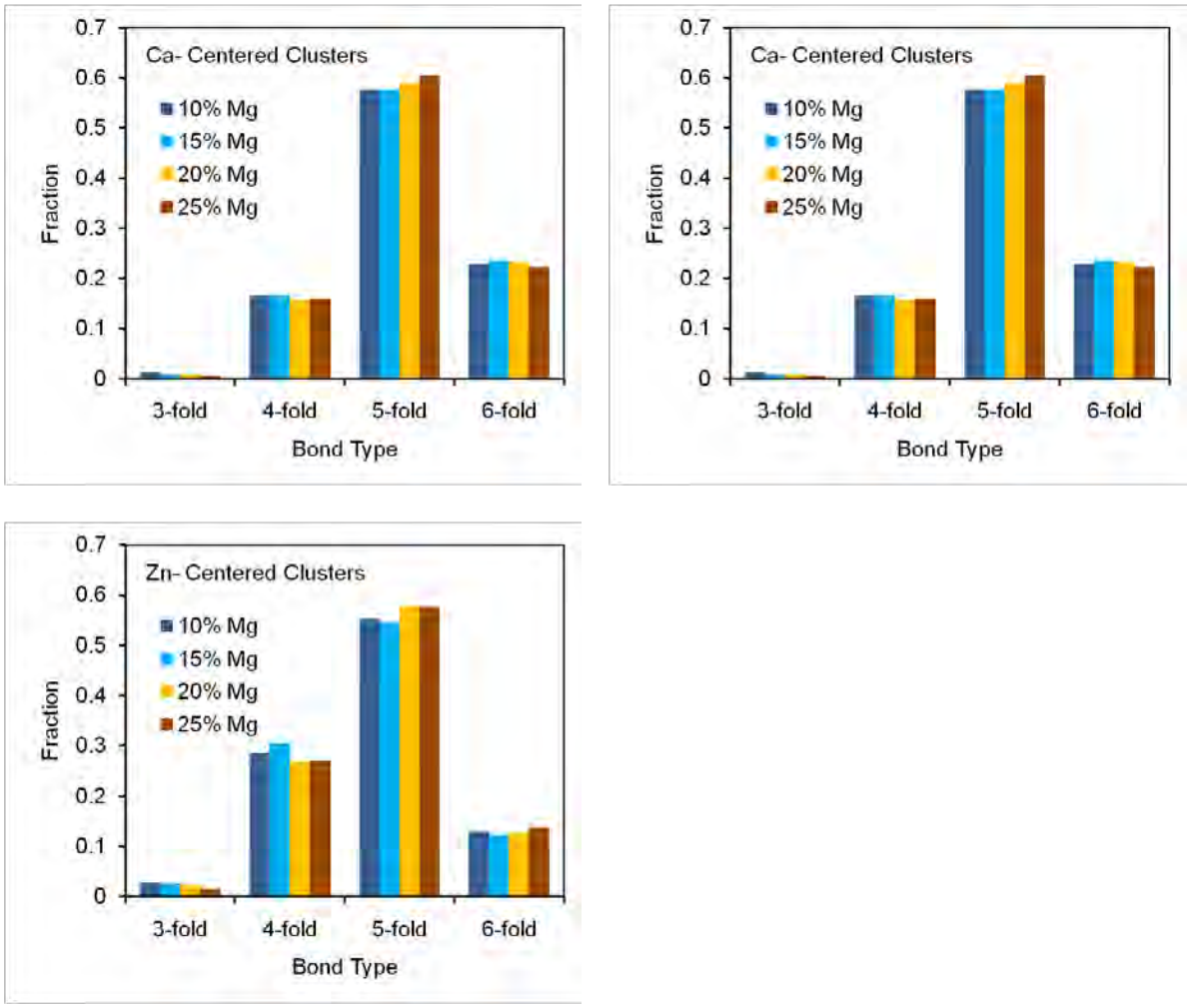

Figure 11 shows the fraction of 3-, 4-, 5- and 6- fold bond vertices in the Ca-, Mg-, and Zn-centered clusters. In all three cluster types, the vertex coordination m = 5 prevails. Domination of polyhedra with 4-, 5-, and 6- bond vertices has been shown [23,20] to be indication of dense atomic packing of the amorphous structure. Moreover, high fraction of 5-bond vertices can indicate domination of pentagonal bi-pyramids as structural units in the amorphous structure. It is worth to note that two pentagonal bipyramids with a common 5-fold vertex connected by ten

tetrahedrons with common faces form a coordination icosahedron, which is believed to be most common cluster in a densely packed amorphous structure [25].

Bond Angle Distributions

The bond angle distributions can provide additional information about most common local structures around the cluster vertices, because characteristic vertex angles are very sensitive to the vertex type (e.g. number and length distributions of vertex bonds).

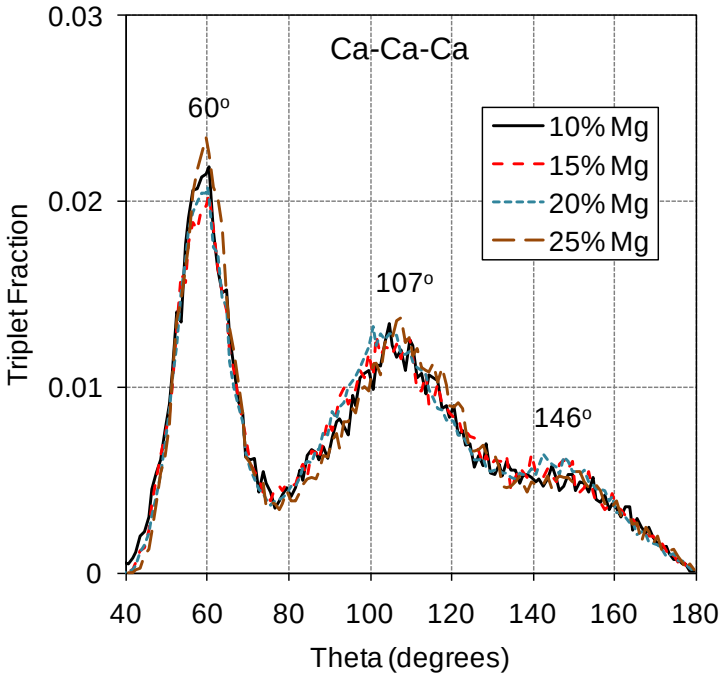

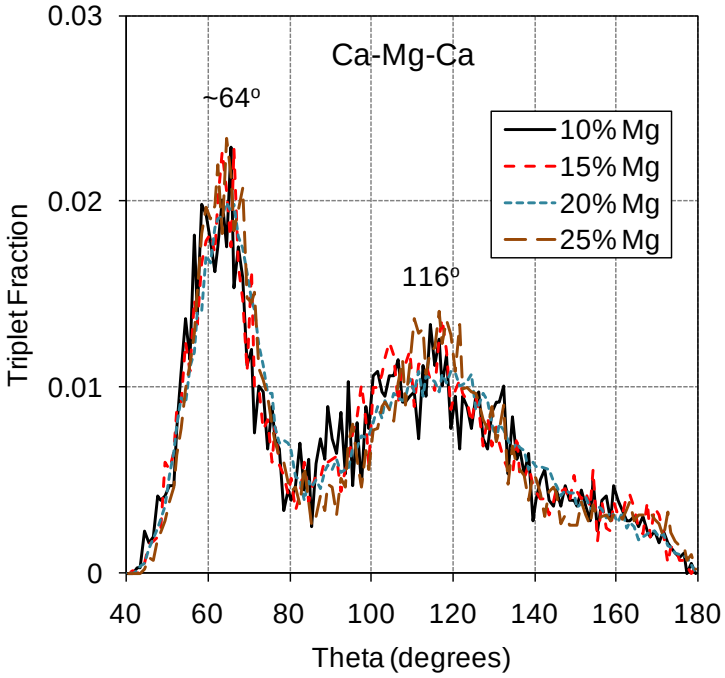

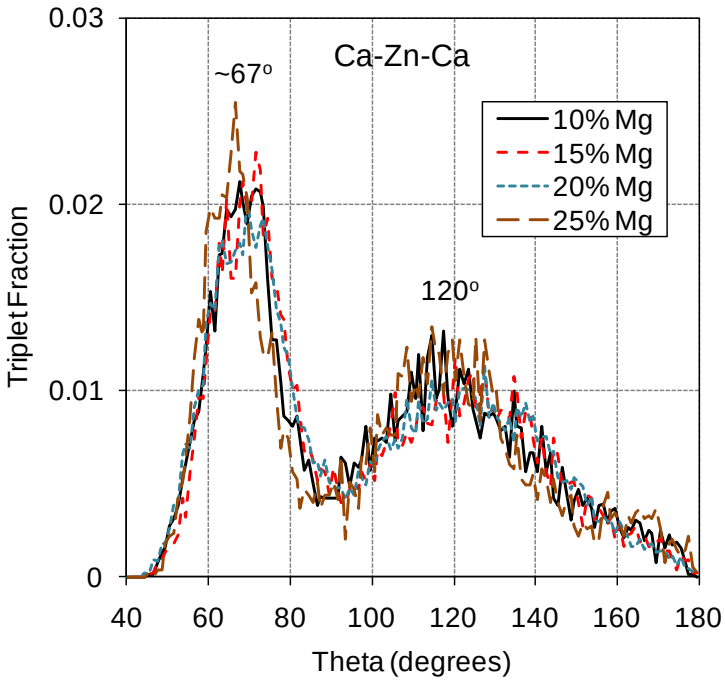

Figure 12 shows Ca-Ca-Ca, Ca-Mg-Ca and Ca-Zn-Ca bond angle distributions in the Ca-Mg-Zn amorphous structures. The upper limit of the bond lengths has been set to 4.6 Å, which corresponds to the end of the first peak of the total RDFs. A characteristic feature for all four

alloys is the first peak located near 60°. The exact 60° angle position for the Ca-Ca-Ca triplets corresponds to the close packing of three equal hard spheres and forming equilateral triangles. For the Mg- and Zn- centered triplets (i.e. Ca-Mg-Ca and Ca-Zn-Ca, the first peak is located at ~64° and 67-69°, respectively. These shifts of the first peak angle position to the higher values can be explained by the smaller atomic radii of Mg and Zn atoms. From the known bond angle values, the effective (most common) bond distance ratios are estimated to be $r_{Ca\text{-}Mg}/r_{Ca\text{-}Ca} = 0.94$ and $r_{Ca\text{-}Zn}/r_{Ca\text{-}Ca} = 0.89$, which leads to the effective atomic radius ratios of $(r_{Mg}/r_{Ca})_{\text{eff}} = 0.88$ and $(r_{Zn}/r_{Ca})_{\text{eff}} = 0.78$. These calculated radius ratios are higher than the metallic radius ratios, $(r_{Mg}/r_{Ca})_{\text{m}} = 0.81$ and $(r_{Zn}/r_{Ca})_{\text{m}} = 0.68$, and covalent radius ratios, $(r_{Mg}/r_{Ca})_{\text{c}} = 0.80$ and $(r_{Zn}/r_{Ca})_{\text{c}} = 0.69$, both are taken from Table 3. The observed Ca-Mg-Ca and Ca-Zn-Ca triplet configurations can be explained by larger shrinking of Ca-Ca bonds than Ca-Mg and Ca-Zn bonds (relative to the respective metallic bond distances), which is in agreement with the weighted bond distances data reported in Table 6.

The second bond angle distribution peak, which is located near 107° for Ca-Ca-Ca triplets, corresponds to the interior angle of 108° of a regular pentagon. A slightly smaller value is probably due to slight distortion of the pentagon, when one of the five Ca atoms in the pentagon vertices is replaced by Mg and/or Zn. Due to shorter Ca-Mg (or Ca-Zn) bonds, the interior angle at the Mg (Zn) vertex of the pentagon increases at the expense of other interior angles, the total sum of which in the pentagon is 540°. Indeed, the second peak for Ca-Mg-Ca and Ca-Zn-Ca triplets is located at ~116° and ~120°, respectively. Having a pentagon consisting of 4 Ca atoms and one Mg/Zn atom and using these values of the interior angle at the Mg/Zn vertex, the interior angles at the other four Ca vertices are calculated to be 106°/105°. To obtain the average angle of

107° for the Ca-Ca-Ca triplets, it should be assumed that one Mg/Zn atom replaces every tenth/fifteenth Ca atom in the pentagon configurations presented in the amorphous structure. The two characteristic peaks in the bond angle distributions that correspond to the angles at the vertices of equilateral triangles and pentagons support our earlier conclusion that tetragons and pentagonal bipiramids are the most common atom configurations in the $Ca_{60}Mg_XZn_{40-X}$ amorphous alloys.

CONCLUSIONS

1. Using combination of neutron and X-ray scattering and Reverse Monte Carlo modeling allowed us to model the amorphous structure of $Ca_{60}Mg_XZn_{40-X}$ alloys and extract partial distribution functions (PDF), which describe well experimental neutron and X-ray structure factors and total correlation functions of these alloys.
2. Amorphous structure of Ca-Mg-Zn BMGs can be described as a mixture of Mg- and Zn-centered clusters, with Ca dominating in the first coordination shell of these clusters.
3. CN = 10 [~7 Ca + 3 (Mg+Zn)] is most common for Zn-centered clusters.
4. CN = 11 and 12 [~7-8 Ca + 4 (Mg+Zn)] are most common for Mg-centered clusters.
5. 5-fold bond configurations (pentagonal pyramids) dominate (~60%) in the first coordination shell of the clusters, suggesting densely atomic packing.
6. Bond angle distributions suggest the near-equilateral triangles and pentagonal bi-pyramids to be the most common atom configurations.
7. Two Ca-Mg-Zn alloys with inferior GFA have increased amounts of (0,0,12,0), (0,2,8,1), (0,2,8,2) and (0,4,4,3) clusters, which suggests that these clusters may facilitate crystallization.

ACKNOWLEDGEMENTS

Technical support from Mr. J. Michael Scott and Dr. Michael Braginsky and extensive discussions with Dr. Alex Kolesnikov and Dr. Wojtek Dmowski are recognized. Experiments at the ISIS Pulsed Neutron and Muon Source were supported by a beamtime allocation from the Science and Technology Facilities Council. Work at AFRL was supported through the Air Force Office of Scientific Research (Dr. Joan Fuller, Program Manager) and the Air Force on-site contract No. FA8650-10-D-5226 conducted through UES, Inc. Dayton, Ohio.

TABLES

Table 1. Density (in g/cm^3 and atoms per Å^3) of Ca-Mg-Zn amorphous alloys produced in this work.

Alloy	Density	
	g/cm^3	Å^{-3}
$Ca_{60}Mg_{10}Zn_{30}$	2.4481 ± 0.0058	0.031985
$Ca_{60}Mg_{15}Zn_{25}$	2.2890 ± 0.0073	0.031301
$Ca_{60}Mg_{20}Zn_{20}$	2.1499 ± 0.0024	0.030837
$Ca_{60}Mg_{25}Zn_{15}$	2.0043 ± 0.0044	0.030227

Table 2. The interatomic bond distances (r_{ij}, in Å), which correspond to the position of the first peak in respective partial PRDFs of the $Ca_{60}Mg_XZn_{40-X}$ amorphous alloys. The bond distance values averaged for four alloys, $(r_{ij})_{aver}$, as well as the deviations of these values from metallic, r_m, and covalent, r_c, bond distances (see Table 3), are also given here.

r_{ij}, Å	$r_{Ca\text{-}Ca}$	$r_{Ca\text{-}Mg}$	$r_{Ca\text{-}Zn}$	$r_{Mg\text{-}Mg}$	$r_{Mg\text{-}Zn}$	$r_{Zn\text{-}Zn}$
$Ca_{60}Mg_{10}Zn_{30}$	3.82	3.44	3.14	3.02	3.02	2.66
$Ca_{60}Mg_{15}Zn_{25}$	3.80	3.48	3.19	3.06	2.78	2.56
$Ca_{60}Mg_{20}Zn_{20}$	3.84	3.48	3.21	3.02	2.84	2.56
$Ca_{60}Mg_{25}Zn_{15}$	3.81	3.52	3.16	3.09	2.85	2.63
$(r_{ij})_{aver}$	3.82	3.48	3.18	3.05	2.87	2.60
$100\%(r_{aver}/r_m\text{-}1)$	-3.1	-2.5	-4.1	-4.8	-2.3	-2.9
$100\%(r_{aver}/r_c\text{-}1)$	8.5	9.8	6.5	8.1	9.2	6.7

Table 3. Metallic, r_m, [26] and covalent, r_c, [27] bond distances (in Å) between Ca, Mg and Zn atom pairs.

	Ca-Ca	Ca-Mg	Ca-Zn	Mg-Mg	Mg-Zn	Zn-Zn
r_m (Å)	3.94	3.57	3.31	3.20	2.94	2.68
r_c (Å)	3.52	3.17	2.98	2.82	2.63	2.44

Table 4. The covalent fraction, f_c, of Ca-Ca, Ca-Mg, Ca-Zn, Mg-Mg, Mg-Zn, and Zn-Zn bonds in four Ca-Mg-Zn amorphous alloys.

f_c	Ca-Ca	Ca-Mg	Ca-Zn	Mg-Mg	Mg-Zn	Zn-Zn
$Ca_{60}Mg_{10}Zn_{30}$	0.29	0.33	0.52	0.47	0.00	0.08
$Ca_{60}Mg_{15}Zn_{25}$	0.33	0.23	0.36	0.37	0.52	0.50
$Ca_{60}Mg_{20}Zn_{20}$	0.24	0.23	0.30	0.47	0.32	0.50
$Ca_{60}Mg_{25}Zn_{15}$	0.31	0.13	0.45	0.29	0.29	0.21
$(f_c)_{aver}$	0.29	0.23	0.41	0.40	0.28	0.32

Table 5. Characteristic bond distances in several binary intermetallic phases.

r (A)	r_{Ca-Ca}	r_{Ca-Mg}	r_{Ca-Zn}	r_{Mg-Mg}	r_{Mg-Zn}	r_{Zn-Zn}
$CaMg_2$	3.81	3.62		3.05 3.13 3.18		
Ca_3Zn	3.78 3.88 3.91 3.95 4.15 4.32		3.18 3.18 3.56 4.17			4.15
CaZn	3.90 4.05 4.20		3.18 3.22			2.62

$MgZn_2$				3.17	3.04	2.53 2.61 2.64
Ca_5Zn_3	3.61 3.76 4.07 4.19		3.14 3.29 3.34			2.69
Minimum	**3.61**	**3.62**	**3.14**	**3.05**	**3.03**	**2.53**
Maximum	**4.32**	**3.62**	**4.17**	**3.18**	**3.04**	**4.15**

Table 6. Weighted bond distances, $r_{ij}^{weighted}$ (in Å), between the atom pairs within the first peak of the total RDFs (the first coordination shell) of the $Ca_{60}Mg_XZn_{40-X}$ amorphous alloys. The bond distance values averaged for four alloys, as well as the difference between the calculated weighted and the first peak bond distances (taken from Table 2) are also given in two last rows.

$r_{ij}^{weighted}$, Å	Ca-Ca	Ca-Mg	Ca-Zn	Mg-Mg	Mg-Zn	Zn-Zn
$Ca_{60}Mg_{10}Zn_{30}$	3.83	3.55	3.32	3.35	3.20	3.21
$Ca_{60}Mg_{15}Zn_{25}$	3.85	3.57	3.29	3.40	3.33	3.30
$Ca_{60}Mg_{20}Zn_{20}$	3.85	3.53	3.35	3.44	3.34	3.36
$Ca_{60}Mg_{25}Zn_{15}$	3.85	3.52	3.43	3.43	3.19	3.38
$r_{ij}^{weighted}$ average	3.84	3.54	3.35	3.40	3.26	3.31
$r_{ij}^{weighted} - r_{ij}$, Å	-0.10	-0.03	0.04	0.20	0.32	0.63

FIGURES

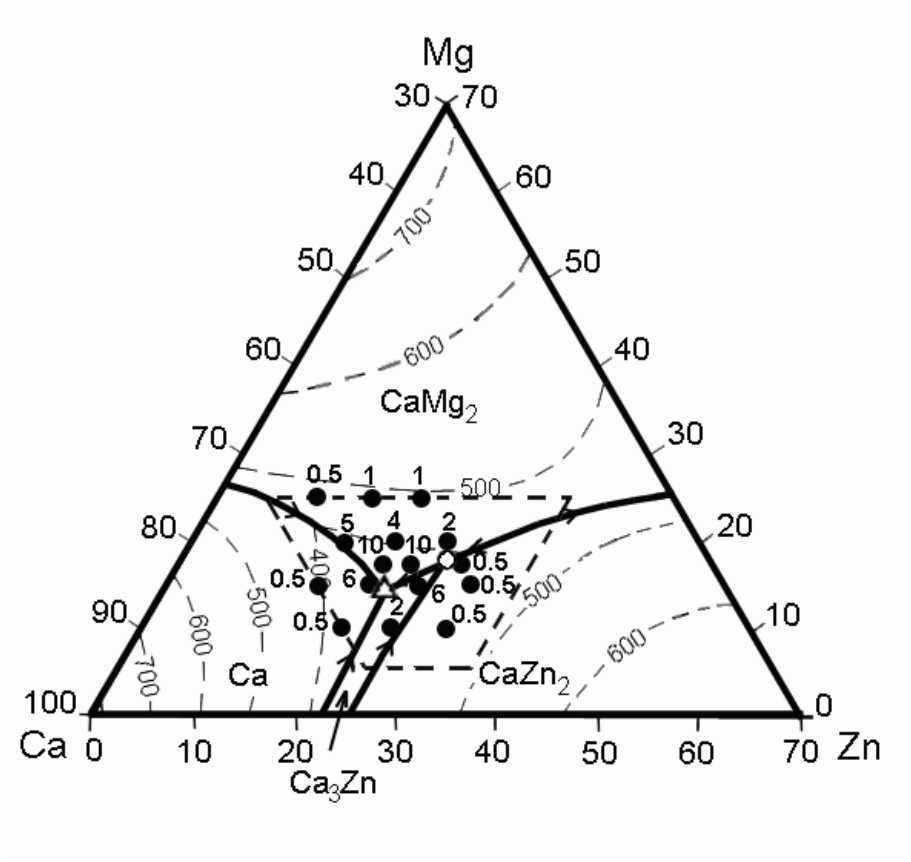

Figure 1. Liquidus projection of Ca-Mg-Zn ternary system. The projection shows dashed isothermal lines and corresponding liquidus temperatures (in ^{o}C) and thick solid lines bounding Ca, $CaMg_2$, CaZn, and Ca_3Zn phase fields. Ternary eutectic and peritectic compositions are marked by an open triangle and an open circle, respectively. The compositions of amorphous alloys and their maximum plate thicknesses (in mm) are shown as solid circles and pertinent numbers. A trapezoid with a dashed boundary represents a composition range for the ternary Ca-Mg-Zn BMGs, in accord to [4].

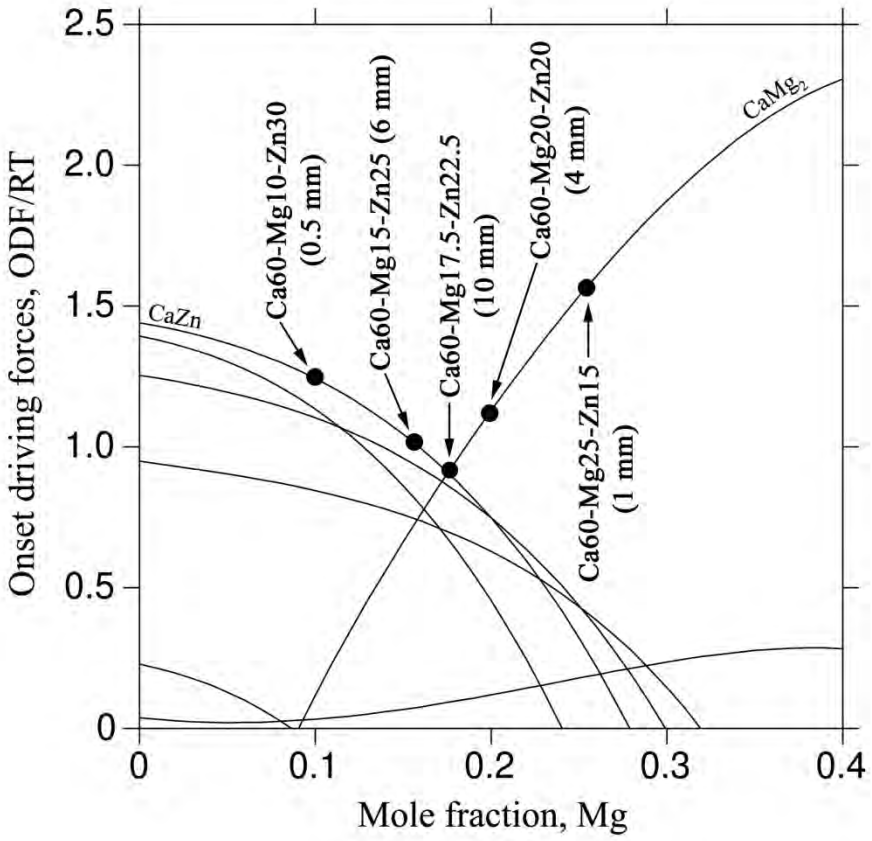

Figure 2. Calculated onset driving forces of various crystalline phases for $Ca_{60}Mg_xZn_{40-x}$ alloys versus Mg content at 390 K. The circles represent the amorphous alloy compositions with indicated critical thicknesses. [10]

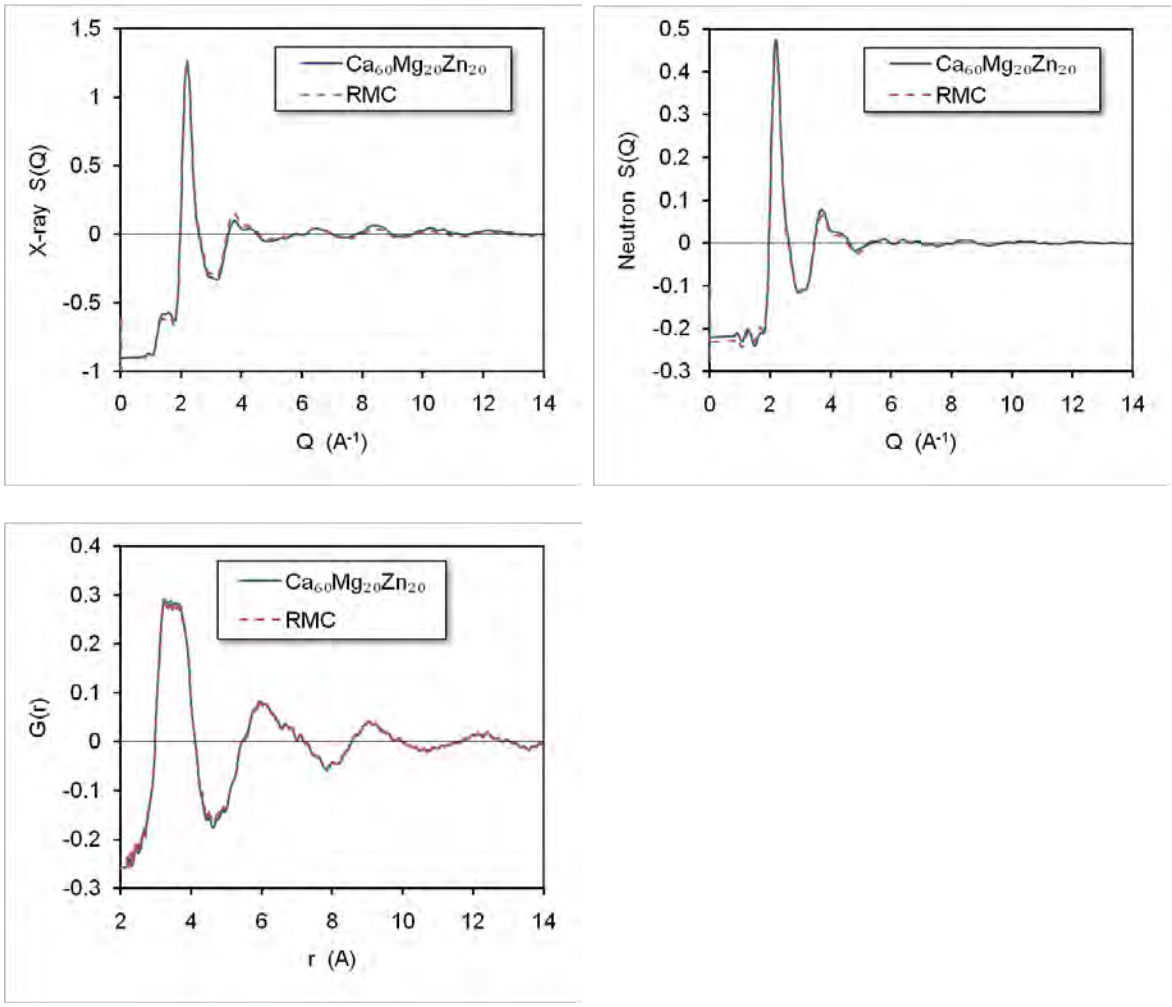

Figure 3. Experimental and RMC simulated X-ray and neutron total scattering structure factors S(Q) and neutron total radial distribution function G(r) for a $Ca_{60}Mg_{20}Zn_{20}$ amorphous alloy.

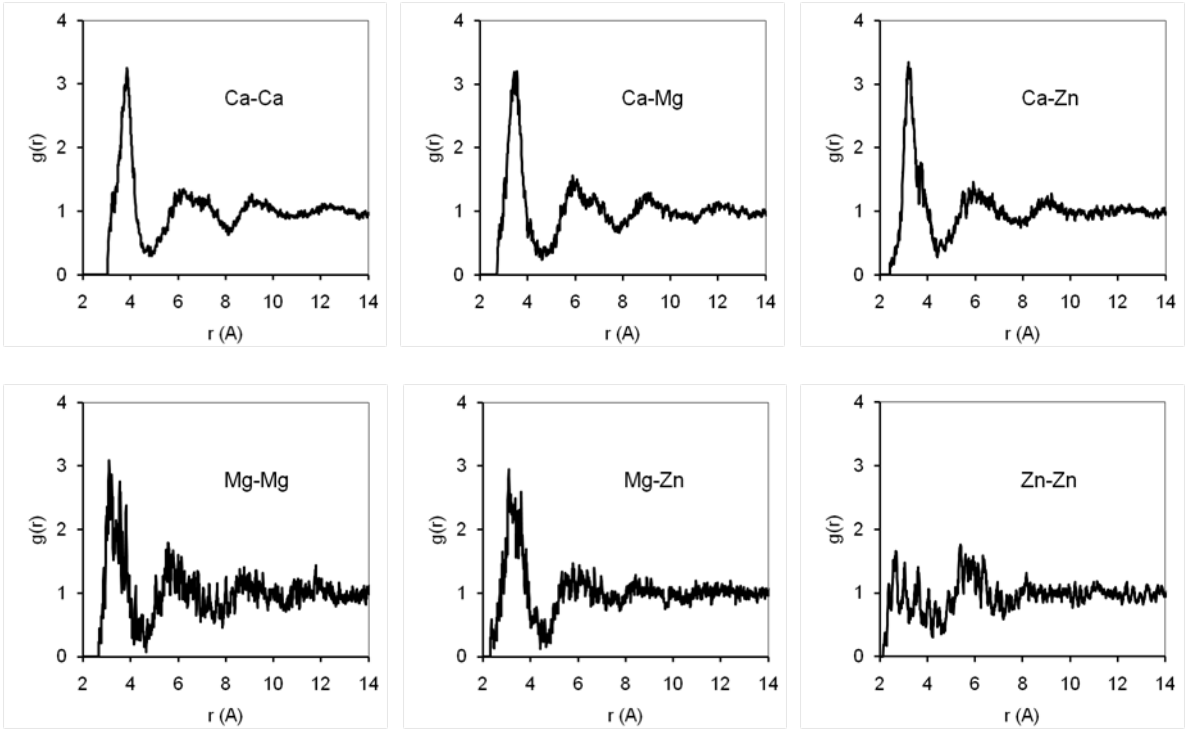

Figure 4. Partial radial distribution functions g(r) for Ca-Ca, Ca-Mg, Ca-Zn, Mg-Mg, Mg-Zn and Zn-Zn atomic pairs in a $Ca_{60}Mg_{20}Zn_{20}$ amorphous alloy.

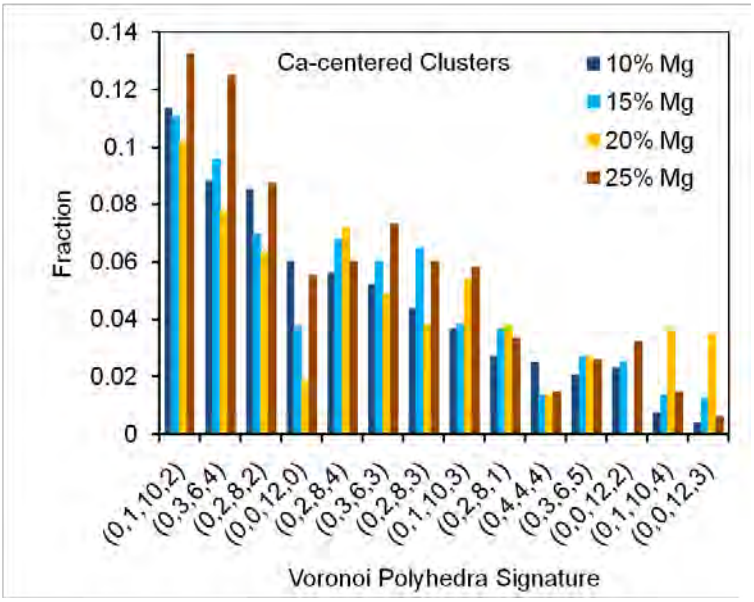

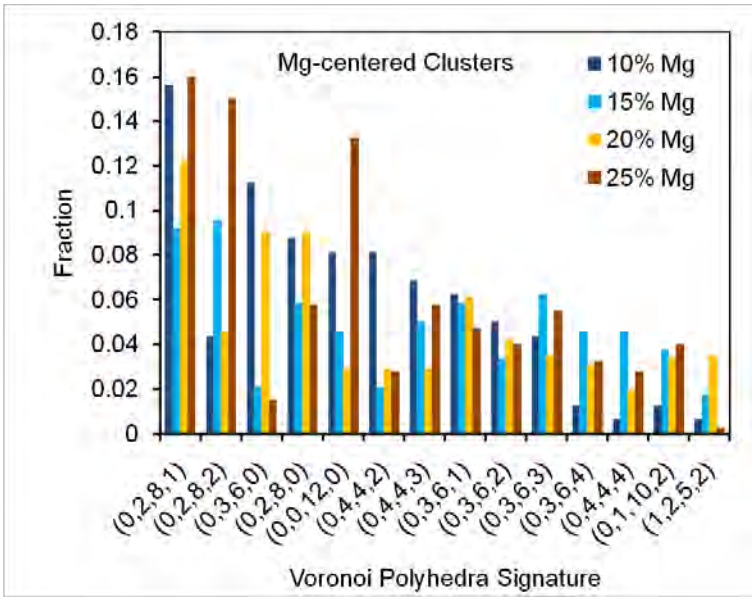

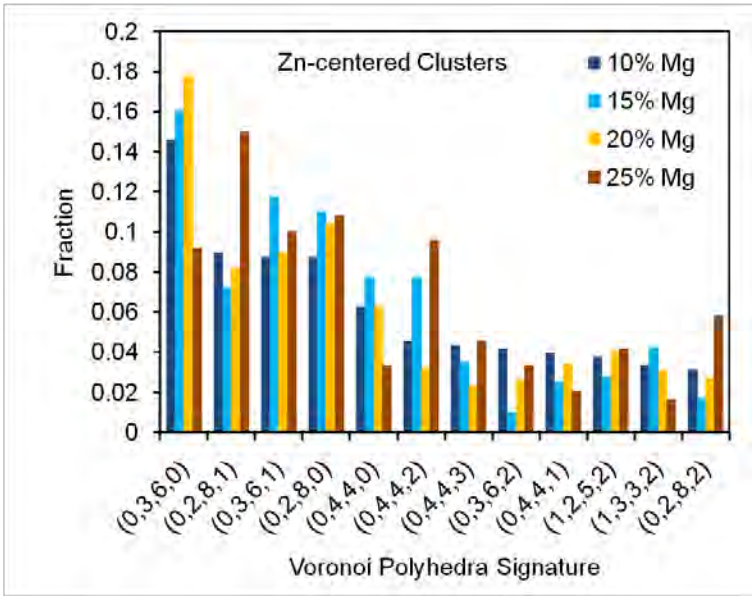

Figure 5. Types of Ca-, Mg-, and Zn- centered clusters and their fractions in four $Ca_{60}Mg_XZn_{40-X}$ amorphous alloys.

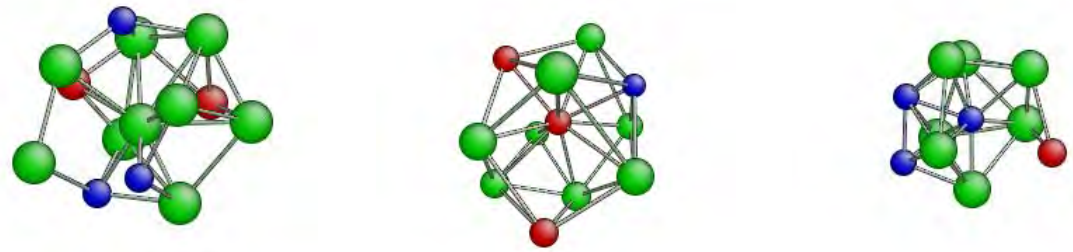

(a) (b) (c)

Figure 6. Configurations of three typical (a) Ca-centered (0,1,10,2), (b) Mg-centered (0,2,8,1), and (c) Zn-centered (0,3,6,1) clusters in the $Ca_{60}Mg_XZn_{40-X}$ amorphous alloys.

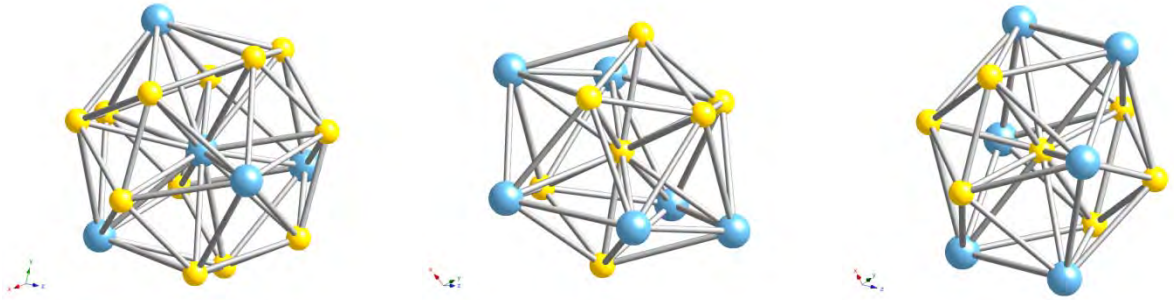

(a) (b) (c)

Figure 7. (a) Ca-centered (0,0,12,4) and (b, c) Mg-centered, both are (0,0,12,0), coordination polyhedra in the $CaMg_2$ crystal structure.

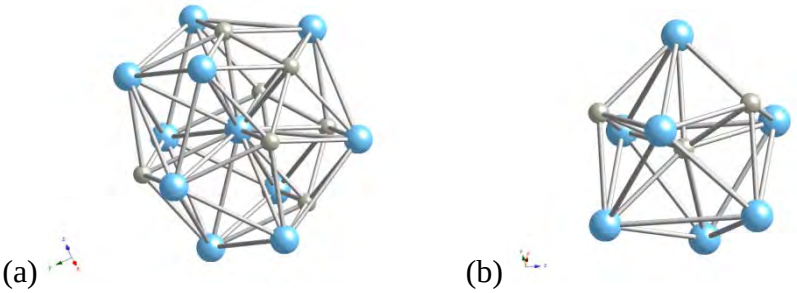

(a) (b)

Figure 8. (a) Ca-centered (0,1,10,6) and (b) Zn-centered (0,3,6,0) coordination polyhedra in the CaZn crystal structure. []

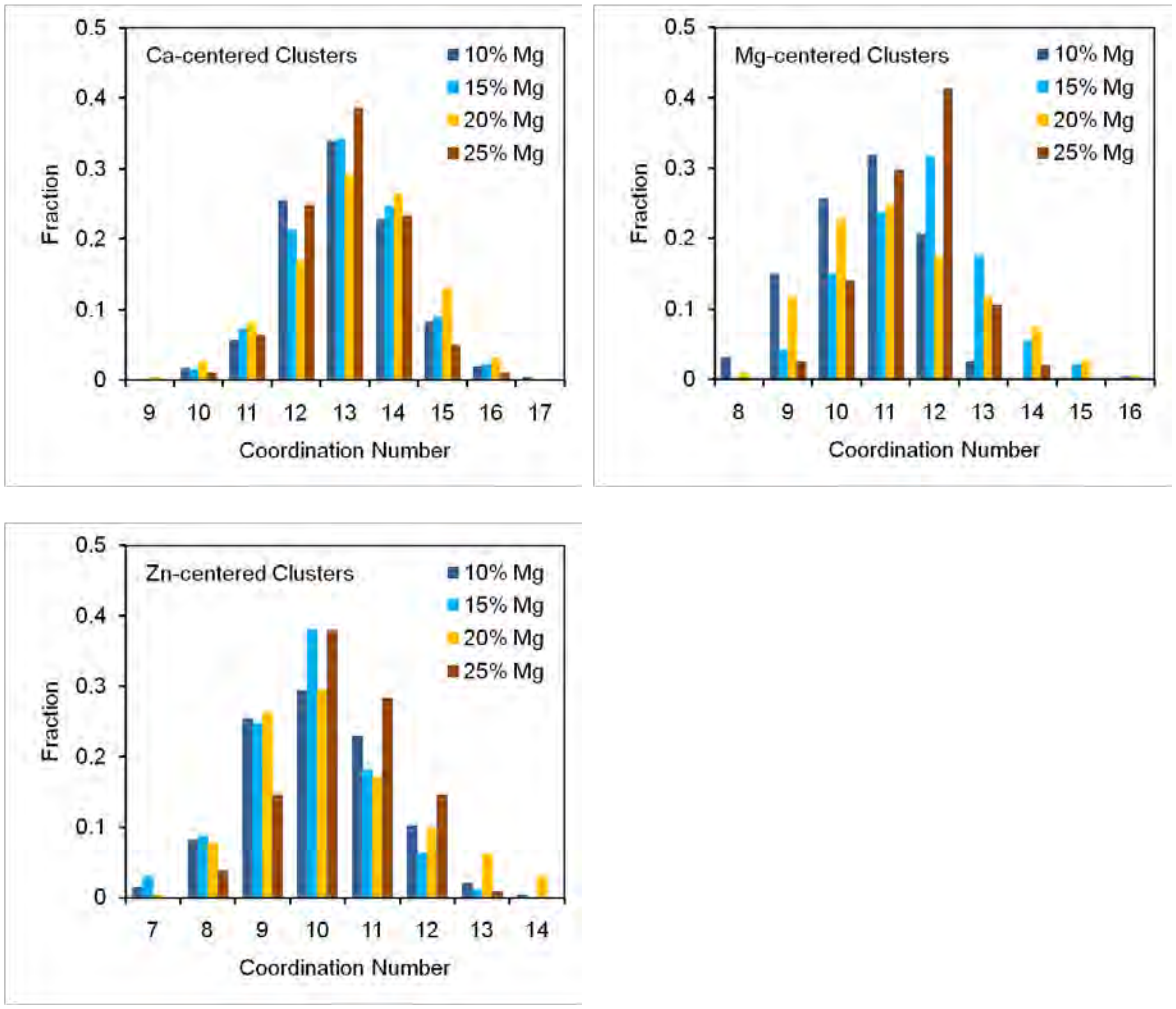

Figure 9. Distributions of Ca-centered, Mg-cantered, and Zn-centered clusters by their total coordination numbers in four $Ca_{60}Mg_XZn_{40-X}$ amorphous alloys.

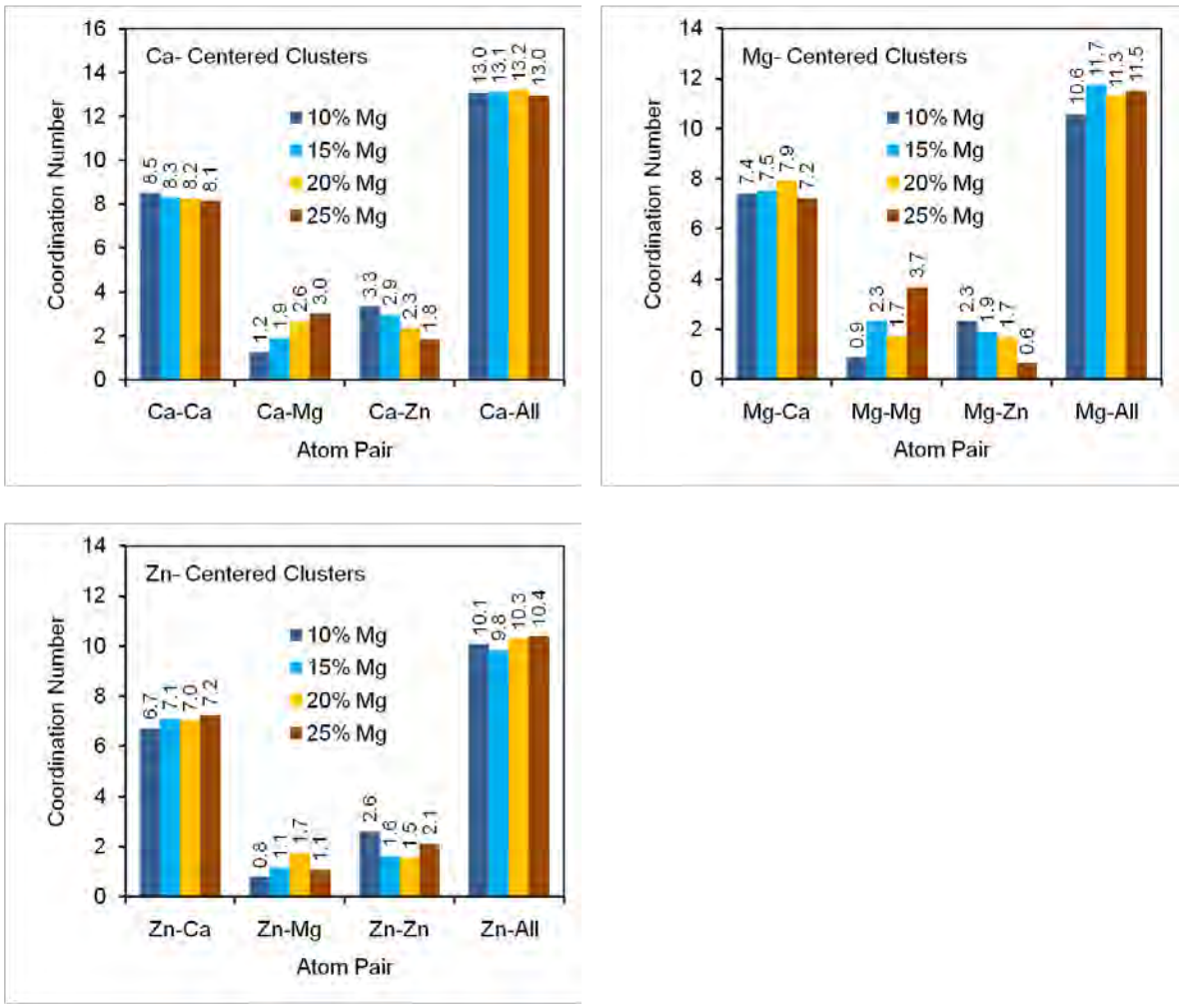

Figure 10. Partial coordination numbers in $Ca_{60}Mg_XZn_{40-X}$ amoprhous alloys as functions of Mg content.

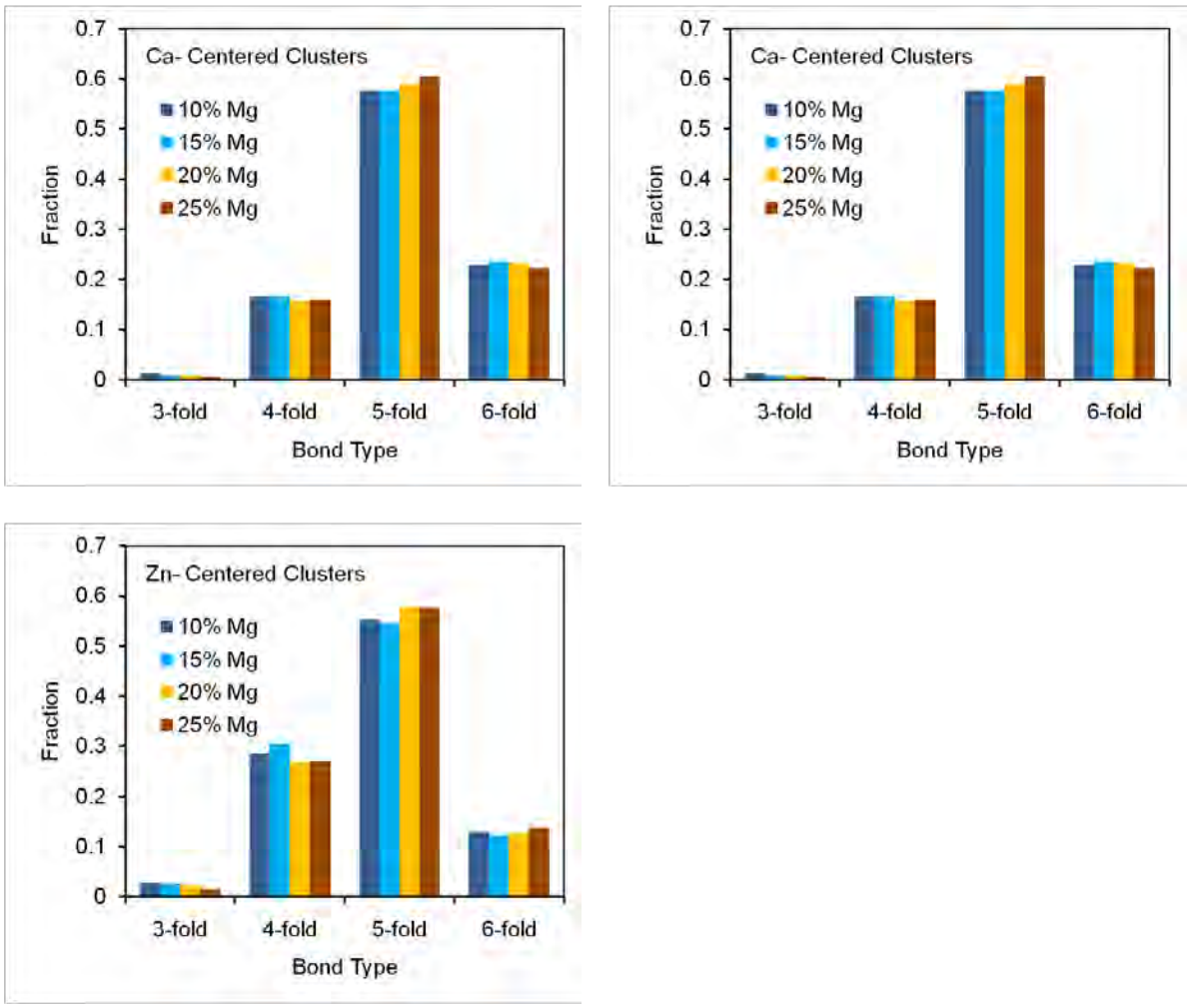

Figure 11. Fraction of vertices with 3, 4, 5, and 6 neighbor atoms (bonds) in Ca-, Mg-, and Zn-centered clusters in four $Ca_{60}Mg_XZn_{40-X}$ amorphous alloys.

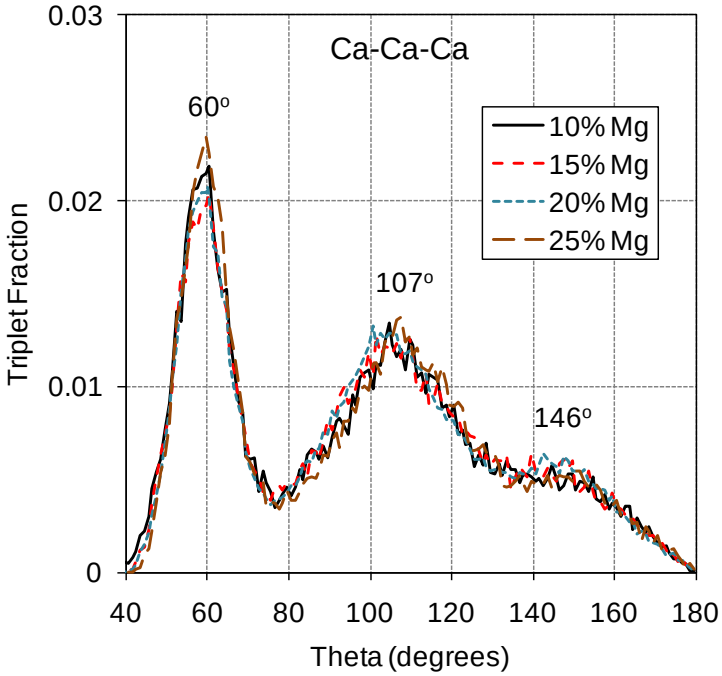

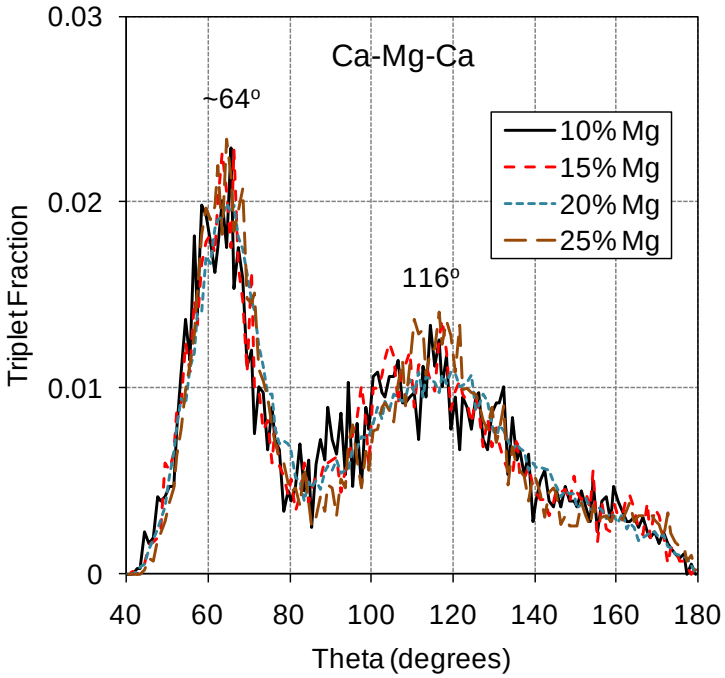

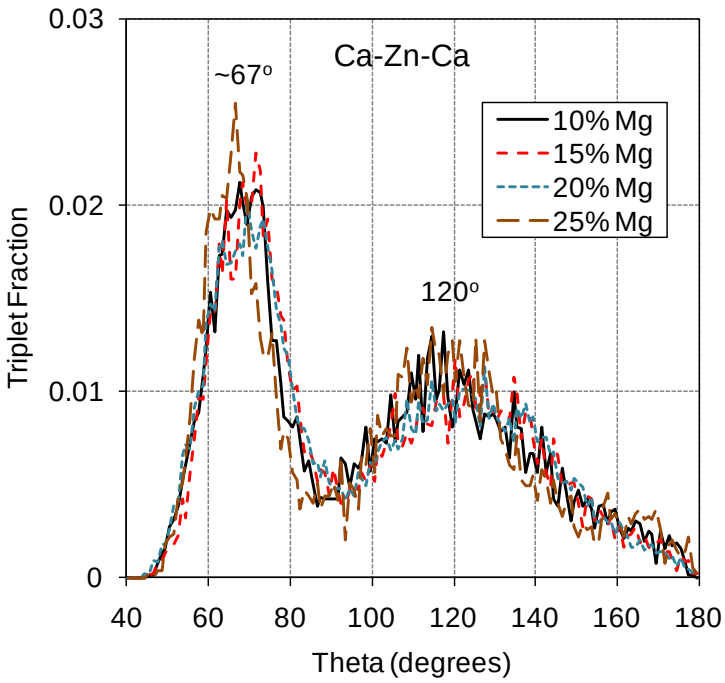

Figure 12. Ca-Ca-Ca, Ca-Mg-Ca and Ca-Zn-Ca bond angle distributions in $Ca_{60}Mg_XZn_{40-X}$ amorphous alloys. A pentagonal pyramid with two characteristic peak bond angles is shown in the insert and represents the most common configuration in the first coordination shell.

REFERENCES

1. O.N. Senkov, J.M. Scott, Scripta Mater. 50 (2004) 449-452.
2. O.N. Senkov, J.M. Scott, J. Non-Cryst. Solids, 351 (2005) 3087-3094.
3. O.N. Senkov, J.M. Scott, D.B. Miracle, J. Alloys & Comp., 424 (2006) 394-399.
4. O.N. Senkov, J.M. Scott, D.B. Miracle, Intermetallics 14 (2006) 1055-1060.
5. O.N. Senkov, J.M. Scott, D.B. Miracle, Materials Trans. 48 (2007) 1610-1616.
6. O.N. Senkov, D.B. Miracle, V. Keppens, P.K. Liaw, Metall. Mater. Trans. A, 39 (2008) 1888-1900.
7. V. Keppens, Z. Zhang, O.N. Senkov, D.B. Miracle, Phil. Mag. 87 (2007) 503-508; V. Keppens, Z. Zhang, O.N. Senkov, D.B. Miracle, Mater. Sci. Eng. 87 (2007) 503-508.
8. O.N. Senkov, D.B. Miracle, Metall. Mater. Trans. A, Published online 3 September 2009; DOI: 10.1007/s11661-009-9981-3.
9. P. Villars, A. Prince, H. Okamoto (Eds.) Handbook of Ternary Alloy Phase Diagrams, Materials Park, OH, ASM International, 1995, p. 7522.
10. S. Gorsse, G. Orveillon, O.N. Senkov, D.B. Miracle, Physical Review B, 73 (2006) 224202/1-9.
11. O.N. Senkov, D.B. Miracle, Mater. Res. Bull. 36 (2001) 2183-2193; D.B. Miracle, W.S. Sanders, O.N. Senkov, Phil. Mag. A, 83 (2003), 2409-2428.
12. D.B. Miracle, Nature Mater., 3 (2004) 697-702; Acta Mater., 54 (2006) 4317-4336.
13. O.N. Senkov, D.B. Mircale, In: Processing and Fabrication of Advanced Materials XIV, T.S. Srivatsan, R.A. Varin, R. Abbaschian, S. Viswanathan (eds.), Materials Science and Technology, Pittsburgh, PA, 2005, pp. 249-266.
14. D.A. Keen, Applied Crystallography, 34 (2001) 172-177.
15 R.L. McGreevy, J. Phys.: Cond. Matter. 13 (2001) R877-R913.
16 D.A. Keen, R.L. McGreevy, Nature, 344 (1990) 423-442.
17 J.L.C. Daams, P. Villars, J.H.N. van Vucht, Atlas of Crystal Structure Types for Intermetallic Phases, Vols. 1-4, ASM International, Materials Park, OH, USA, 1991.
18 R. Zallen, The Physics of Amorphous Solids, Wiley-VCH, Weinheim, 2004.
19 J.D. Bernal, Proc. R. Soc. A 280 (1964) 299-322.
20 D.R. Nelson, Phys. Rev. B 28 (1983) 5515-5535.

21 Evan Ma, Nature paper

22 J.L. Finney, Proc.R.Soc. A 319(1970) 495-507.

23 F.C. Frank, J.S. Kasper, Acta Crystallogr. 11 (1958) 184-190.

24 D.B. Miracle, W.S. Sanders, O.N. Senkov, Philos. Mag. 83 (2003) 2409-2428.

25 A.S. Clarke, H. Jonsson, Phys. Rev. E 47 (1993) 3975-3984.

26 N.N. Greenwood, A. Earnshaw, Chemistry of the Elements (2nd ed.), Butterworth-Heinemann, Oxford, UK, 1997

27 B. Cordero, V. Gómez, A.E. Platero-Prats, M. Revés, J. Echeverría, E. Cremades, F. Barragán and S. Alvarez. Covalent Radii Revisited. Dalton Trans., 2008, 2832-2838, doi: 10.1039/b801115j.